

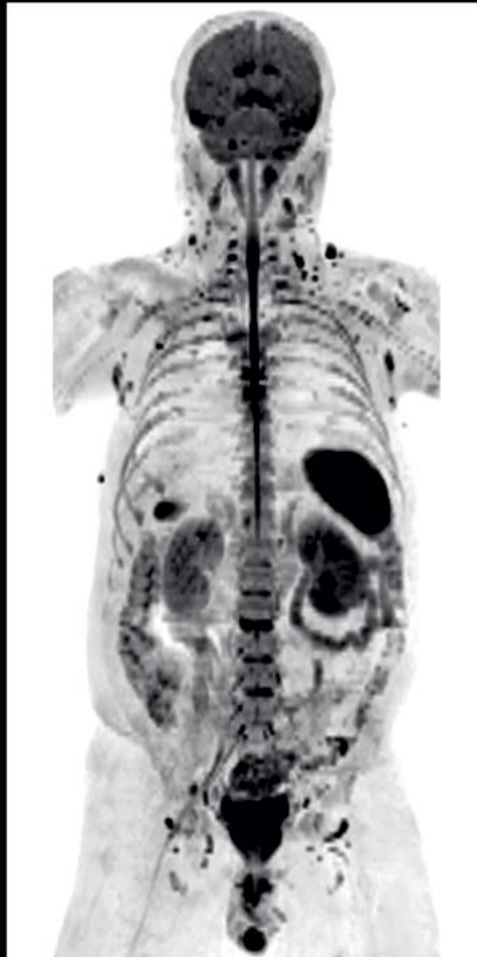
Editorial Comment
Konstantin Nikolaou
Page 2

CoilShim
Miriam R. Keil
Page 11

SliceAdjust
Xue Huadan
Page 17

Whole-Body Dot Engine
Căcilia Reiner
Page 22

syngo MR XA10
Gregor Thörmer
Page 32



Cover images MAGNETOM Vida



MAGNETOM Flash

MAGNETOM Vida and BioMatrix special issue



Professor
Konstantin
Nikolaou

Konstantin Nikolaou is Chairman of the Department of Diagnostic and Interventional Radiology in the Department of Radiology at the Eberhard-Karl-University in Tübingen, Germany. Professor Nikolaou received his MD from the Ludwig-Maximilians-University of Munich, Germany, in the year 2000, where he also became an Assistant Professor at the Department of Clinical Radiology, University Hospitals Munich, after finalizing his PhD-thesis on the topic of modern cardiovascular computed tomography techniques in 2007.

After working as a section chief of CT/PET-CT and MRI at the same department, he became Vice Chair of the Department of Clinical Radiology at the Ludwig-Maximilian-University in Munich in April 2007.

Precision Medicine and Adaptive Technologies in Medical Imaging

Dear colleagues, dear readers,

I feel honored and excited to be invited to write an editorial for MAGNETOM Flash on the topic of ‘precision medicine’ – a term that might seem overused these days. Whilst this term is not new – medicine always wants to deliver the right treatment to the right patient at the right time – our understanding of correlations between genome, habits, and diseases is evolving rapidly and exponentially. It feels like there is a need to re-imagine and re-organize health services.

All fields of medicine are adapting to an increasing and increasingly complex demand of phenotyping and genotyping our patients, identifying precise cohorts, and optimizing health care. To us as radiologists, it may seem obvious, that radiology should certainly play a key role in phenotyping these sub-populations by means of dedicated imaging strategies [1]. This should be complementary, and not compete with other ways of phenotyping, including, for example, advanced laboratory tests, histo-pathology, and immunopathology. To integrate our radiological imaging data and reports in a phenotyping system that categorizes patients into well-defined prognostic and therapeutic categories, we will have to learn and adapt to a rising demand of ‘imaging biomarkers’, ‘reproducible parameters’ and ‘standardized’ as well as ‘structured’ reporting.

I am sure our readers are optimistic as I am that we will be able to successfully master these challenges. However, at the same time, we are facing new opportunities and threats,

in terms of increasing economic pressure and increasing workload, ‘value-based’ healthcare, introducing artificial intelligence in clinical routine, and commoditization of imaging procedures and radiological reports [2, 3]. We need clear and concerted strategies to handle these challenges and these include,

- A) accepting and taking on a stronger role of radiologists, as clinical partners and information specialists,
- B) setting new standards in quality and workflows, and
- C) finding answers to an increasing demand of personalization and parametrization in our daily routine.

In this volume of MAGNETOM Flash, exciting views and reports on advancements in MR technologies, enabling us to improve quality, workflows, flexibility, and standardization, clearly reflect these trends and endeavors – in a way that I find very convincing.

1. A new role for radiologists?

Radiologists will have to adapt. And we will have to adapt quickly, to both an increasing economic pressure and to the ‘fourth industrial revolution’, i.e., a rapidly improving process automatization on the basis of big data and artificial intelligence (AI) [4, 5]. The first challenge will be to adapt and re-invent our ever more complex imaging procedures and skills in the era of ‘value-based healthcare’. Since ‘value’ is defined as health or patient outcomes, or

He also is president of the European Society of Molecular and Functional Imaging in Radiology (ESMOFIR) and treasurer for the European Society of Cardiac Imaging (ESCR), Member of the Research Committee of the European Society of Radiology (ESR) and Honorary Member of the Greek Society of Radiology.

Professor Nikolaou joined the Eberhard-Karl-University Tübingen in April 2014 as Chairman of the Department of Diagnostic and Interventional Radiology. His main fields of interest are multimodality and multi-parametric imaging modalities in oncology as well as non-invasive imaging of cardiovascular diseases.



Tübingen, Germany

costs, we should therefore be measured on the results and quality of our care and not on the volumes of service delivered. However, if we agree to enter this circle of optimizing our workflows and outcome-centered care, will we be degraded to delivering standardized services and reports within a (short) given time, i.e., will medical imaging become a commodity? The strength of radiology is not only in the delivery of (automated) results from using sophisticated technologies, but even more by providing an optimized diagnostic process and data integration, provided by dedicated, highly skilled, specialized and communicating colleagues in our field, i.e., radiologists and technicians.

Radiology's value chain has to be high-quality, patient-centered, and results-oriented at the same time. This will enable us to develop from volume-based imaging to value-based imaging, demonstrating the added value of imaging in each phase of patient care and transforming imaging results into measurable metrics (e.g., quantitative imaging results, or cost effectiveness). The primary objective is to maintain and improve our visibility and demonstrating our capabilities as radiologists, imaging experts and highly trained specialists to our clinical partners and patients in daily practice, in our conferences, tumor boards, telephone calls, patient interactions, and interventional procedures. Optimizing our workflows and constant quality-control of our daily work (scheduling, protocols, procedures, reporting, distribution, and communication) is the foundation, basis, and pre-requisite for this, and should be self-evident, but how our report affects therapeutic decisions will directly influence patient outcome and costs of healthcare.

Will this process include an increasing automatization of our reports, at least in parts? Maybe yes. Is this detrimental or dangerous for our field? No, not, if we lead the way and use these new tools to our and our patients' advantage. Even the best trained colleague will not be able to stay perfectly up-to-date with all medical advancements. At the same time, age distribution in our western societies is changing drastically and imaging volumes are steadily

increasing and will continue to do so. Thus, should we not embrace help from technology, rather than to fear it?

There are a number of ways how we could profit from AI. Besides the problem of data, image and information overflow, we will need AI for rare diseases, complex syndromes, or for decision-support systems, to face the growing complexity of our multi-disciplinary, multi-modal, and multi-scale clinical work, combining information from imaging, -omics, lab test, clinical history, and physical exams. The risk is not in the automatization, even of routine reports on frequent imaging procedures such as chest X-rays, mammograms, or CT angiographies to exclude pulmonary embolism. The crucial question will be: Who is in the driver's seat, for technical implementation of these new AI techniques, and for the final decisions. We will have to take action and participate in these developments rather than ignore them, and – if we do it right – we will be able to improve our services and quality. In this process radiologists will transform to information specialists, implementing innovative forms of data handling and data presentation, and focusing on image-guided personalization of our own interventional measures and procedures.

2. New quality standards of radiological services

Multimodal, molecular, and functional imaging is becoming increasingly important in the context of personalized medicine. Our non-invasive diagnostic and imaging procedures are increasingly used to support and complement the data of advanced molecular diagnostics. Complementary qualitative and quantitative imaging parameters play a major role in the assessment of our patients' individual prognosis, the prediction of treatment success and in the monitoring of the therapy effectiveness and outcome. With '-omics' technologies reaching maturity, these will be more and more implemented in clinical practice. Prospective and, where necessary, randomized clinical studies will be needed to validate novel imaging biomarkers, imaging phenotypes, and imaging signatures.

“With recent advances in MR technology, we will optimize workflow and scanning efficiency, while providing consistent, high-quality personalized examination results at the same time, entering a new era in precision medicine.¹”

Professor Konstantin Nikolaou

High quality collections of biological samples procured in a standardized manner from age- and disease-stratified collections coupled to omics- and imaging-based phenotype information are required for the purpose of identification and validation of new, ideally quantitative, imaging biomarkers. By implementing these reproducible, quantitative, and standardized imaging biomarkers, multimodal image information can be integrated with patient-specific data for the development of individualized and predictive disease models.

To reach this goal, examination protocols and image acquisition must be standardized and homogenized as far as possible, in order to achieve a comparability and transferability of results from the various imaging modalities and between different sites. In addition, strategies for a systematic structuring of our reports and findings will have to be implemented, in order to replace the traditional, descriptive reporting of findings. Structured reporting will lead to the possibility of systematic data extraction from our reports, making them more accessible to statistical correlative analyses and bioinformatics. The term ‘structured analysis and reporting’ thus describes the establishment of objective, quantitative, extractable, and reproducible standards, e.g., in the context of tumor-specific diagnostic criteria and follow-up. This results in complete and comprehensive reports and considerably increases the objectivity and comparability between different investigators and sites and at the same time creates the possibility to link these image data with those from molecular diagnostics and to scientifically evaluate them or integrate them in complex disease models. The implementation of standardized vocabularies and reporting rules, supported by radiological lexicons and glossaries, established and disseminated by national and international radiological societies, will further harmonize the use of radiological terms and expressions and will enable optimized indexing of our reports.

3. Adaptive imaging technologies in the era of precision medicine

So how, we may ask, do recent MR developments anticipate these challenges and react to the growing demands described above? Due to high levels of exam complexity, patient properties, and user variability, MRI is still considered to be one of the most complex medical imaging modalities. Innovative MR scanner technology should therefore be able to automatically or semi-automatically address anatomical and physiological differences among individual patients, thus, a wider range of routine scanning procedures as well as complex protocols will be applicable to a larger extent of patients, even those formerly not eligible for MRI examinations, delivering more robust and more consistent results. Also, in times of economic pressure, MR scanning will have to be more cost-effective, by greater robustness and acquisition speed, reducing re-scans and increasing productivity.

To provide our patients with individualized and personalized diagnostic strategies and tailored therapies, we need robust, standardized, and reproducible acquisition techniques that are constantly delivering high and comparable quality. Only then we can compare results and link them with additional information, such as data from laboratory medicine or genetic analyses. Recent technologies will allow us to access new and growing clinical fields – for instance, enabling scans in patients with cardiac arrhythmias, excess weight, or other health problems that prevent them from actively supporting the scan.

An impressive array of various innovative MR technologies will be discussed in this present edition of MAGNETOM Flash. For example, dedicated acceleration techniques implementing Compressed Sensing (GRASP-VIBE) enable dynamic, free-breathing liver examinations in one comprehensive scan by the push of button and for every patient, making breath-holds and complex timing of several dynamic contrast phases unnecessary. Optimized shimming technologies based on new hardware and transmit technologies, such as

CoilShim, one of the BioMatrix Tuners, homogenize the static magnetic field and significantly improve fat saturation and signal exploitation, e.g., in diffusion-weighted imaging (DWI) of body regions difficult to image, such as the neck. Slice-specific shimming (SliceAdjust) is introduced with MAGNETOM Vida as an effective method to reduce susceptibility effects in whole-body DWI at 3T. Automatization of whole-body MR examinations, e.g. the Whole-Body Dot Engine, will significantly reduce overall imaging time, increase patient comfort and will potentially change our use of MRI, e.g., for an increased implementation of whole-body tumor staging. In cardiac imaging, implementation of highly accelerated real-time sequences will preserve diagnostic image quality even in challenging scenarios, such as in arrhythmic patients. Finally, complete free-breathing cardiac examinations will become possible.

The challenges in our field are increasing and may be greater than ever; our clinical and scientific working environment is getting more complex and more demanding. Only if we understand the challenges and take our chances, we will stay in the driver's seat, developing radiology to play an even more central role in clinical care. With recent advances in MR technology, we will optimize workflow and scanning efficiency, while providing consistent, high-quality personalized examination results at the same time, entering a new era in precision medicine.



Konstantin Nikolaou

Editorial Board

We appreciate your comments.
Please contact us at magnetomworld.med@siemens-healthineers.com



Antje Hellwich
Editor-in-chief



Reto Merges
Head of Scientific Marketing



Sunil Kumar S.L., Ph.D.
Senior Manager Applications,
Canada



Wellesley Were
MR Business Development
Manager Australia and
New Zealand



Gary R. McNeal, MS (BME)
Advanced Application Specialist,
Cardiovascular MR Imaging
Hoffman Estates, IL, USA

Review Board

Lisa Chuah, Ph.D.
Global Segment Manager Neurology, Pediatrics, and Orthopedics

Daniel Fischer
Head of Outbound Marketing MR Applications

Berthold Kiefer, Ph.D.
Head of Oncological Applications

Heiko Meyer, Ph.D.
Head of Neuro Applications

Efren Ojeda
MR Marketing Application Center

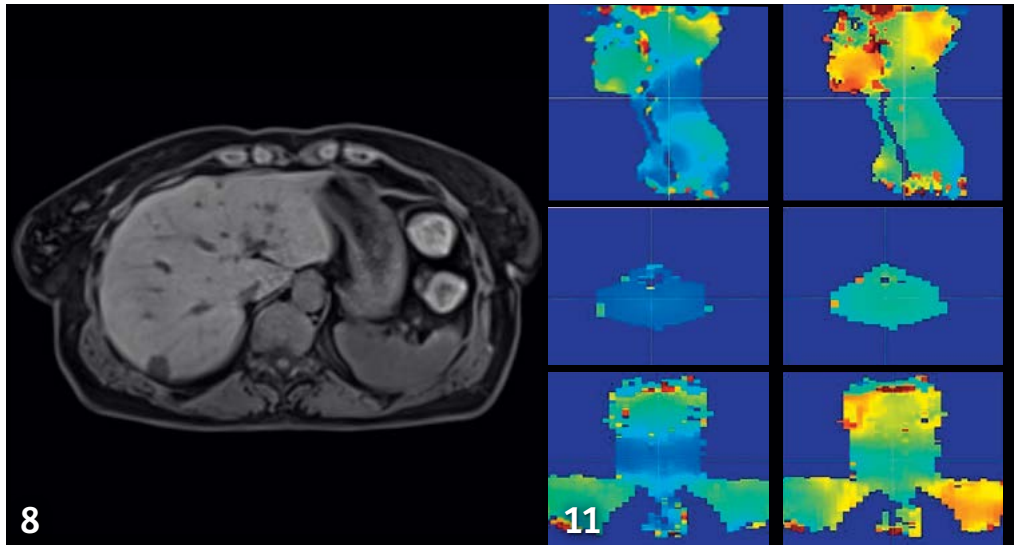
Gregor Thörmer, Ph.D.
Global Segment Manager Men's and Women's Health

References

- ¹Herold CJ, Lewin JS, Wibmer AG, Thrall JH, Krestin GP, Dixon AK, Schoenberg SO, Geckle RJ, Muellner A, Hricak H. Imaging in the Age of Precision Medicine: Summary of the Proceedings of the 10th Biannual Symposium of the International Society for Strategic Studies in Radiology. *Radiology* 2016;279(1):226-238.
- ²Beam AL, Kohane IS. Translating Artificial Intelligence Into Clinical Care. *JAMA* 2016;316(22):2368-2369.
- ³Jha S, Topol EJ. Adapting to Artificial Intelligence: Radiologists and Pathologists as Information Specialists. *JAMA* 2016;316(22):2353-2354.
- ⁴Forsting M. Hot Topics: Will Machine Learning Change Medicine? *J Nucl Med* 2017.
- ⁵Kohli M, Prevedello LM, Filice RW, Geis JR. Implementing Machine Learning in Radiology Practice and Research. *AJR Am J Roentgenol* 2017:1-7.

¹The statements by the Siemens Healthineers customer presented herein are based on results that were achieved in the customer's unique setting. Since there is no "typical" hospital and many variables exist (e.g., hospital size, case mix, level of IT adoption), there can be no guarantee that other customers will achieve the same results.

Contents



8 Free-breathing liver dynamics with Compressed Sensing GRASP-VIBE

11 B₀ field map with and without BioMatrix Tuners: CoilShim



Learn from the experience of other MAGNETOM users

The MAGNETOM World is the community of Siemens Healthineers MR users worldwide, providing you with relevant clinical information. Here you will find application tips and protocols to optimize your daily work. Lectures and presentations from experts in the field will allow you to be exposed to new ideas and alternative clinical approaches.

Put the advantages of the MAGNETOM World to work for you!

siemens-healthineers.us/vida-flash

Editorial Comment

- 2 Precision Medicine and Adaptive Technologies in Medical Imaging**
Konstantin Nikolaou, University Hospital Tübingen, Germany

Image Gallery

- 8 MAGNETOM Vida**
Embrace human nature at 3T. With BioMatrix

Head and Neck Imaging

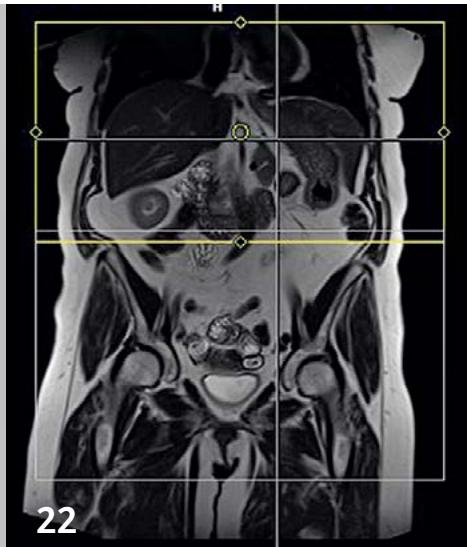
- 11 BioMatrix Tuners: CoilShim**
Miriam R. Keil, et al., Siemens Healthineers, Erlangen, Germany

Whole-body Imaging

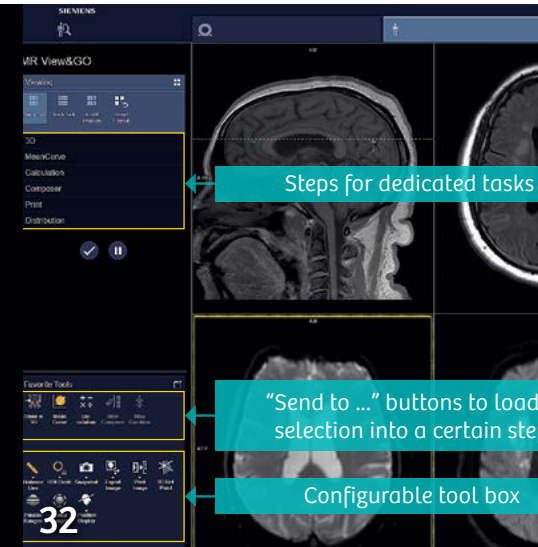
- 17 Slice Specific Shimming Improves the Image Quality of Whole-Body Diffusion-Weighted Examinations at 3T**
Xue Huadan, et al., Peking Union Medical College Hospital, Beijing, China
- 22 Whole-Body Dot Engine: First Clinical Experience with Automated Chest, Abdomen and Pelvis Examinations**
Cäcilia S. Reiner, et al., University of Zurich, Zurich, Switzerland



17 Slice specific shimming for whole-body diffusion-weighted imaging



22 Automated chest, abdomen, and pelvis examinations with Whole-Body Dot Engine



32 syngo MR XA10 for comfortable scanning and intuitive image processing

Technology

- 26 **Compressed Sensing: a Paradigm Shift in MRI**
Christoph Forman, et al., Siemens Healthineers, Erlangen, Germany

Product News

- 32 **syngo MR XA10—Your New Work Environment for More Comfortable Scanning and Intuitive Image Processing**
Gregor Thörmer, et al., Siemens Healthineers, Erlangen, Germany

The information presented in MAGNETOM Flash is for illustration only and is not intended to be relied upon by the reader for instruction as to the practice of medicine. Any health care practitioner reading this information is reminded that they must use their own learning, training and expertise in dealing with their individual patients. This material does not substitute for that duty and is not intended by Siemens Healthineers to be used for any purpose in that regard. The treating physician bears the sole responsibility for the diagnosis and treatment of patients, including drugs and doses prescribed in connection with such use. The Operating Instructions must always be strictly followed when operating the MR System. The source for the technical data is the corresponding data sheets.

MAGNETOM Vida

Embrace human nature at 3T. With BioMatrix

BioMatrix represents a paradigm shift in MRI imaging. MAGNETOM Vida is the first BioMatrix system and the latest 3T Open Bore system.

BioMatrix is a revolutionary new technology, evolving from Tim (Total imaging matrix), and it consists of three unique technologies – BioMatrix Sensors, BioMatrix Tuners, and BioMatrix Interfaces. As part of the BioMatrix Tuners, CoilShim has integrated shimming elements in the Head/Neck Coil to improve B_0 homogeneity, thus enabling excellent results in the c-spine in all patients (Fig. 2). New, ultra-flexible 18-channel surface coils help to consistently deliver excellence in daily clinical routine: faster setup with dedicated positioning devices, shorter exam times with Pat factors up to 3 and higher spatial resolution due to substantially higher SNR than conventional flex coils (Figs. 4, 5). Trendsetting applications for highly accelerated imaging such as Simultaneous Multi-Slice (SMS) and Compressed Sensing strongly benefit from high coil element density in the field-of-view (FOV). By introducing a new Spine 72 coil¹ (12 rows of 6 elements) which can be seamlessly combined with Body 30 coils and the Head/Neck 64 coil it is, for example, possible to perform whole-spine examinations accelerated by a factor of 4 (Fig. 3). Equipped with a new magnet with 55 x 55 x 50 cm FOV, full coverage abdominal scans or long bone exams in one station with excellent fat saturation are feasible (Figs. 6, 7D).

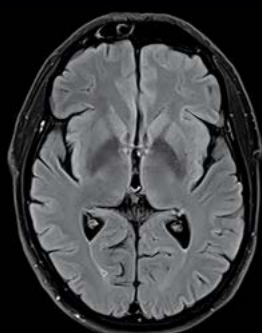
Besides excellent routine clinical capabilities, MAGNETOM Vida is expanding the patient population eligible for MRI. Now, complete free-breathing cardiac examinations are possible with Compressed Sensing Cardiac Cine (Fig. 8) and Extended HeartFreeze. Further planned for MAGNETOM Vida is Compressed Sensing GRASP-VIBE for free-breathing liver



dynamics, improving examinations for children¹, multi-morbid patients, and hearing-impaired patients (Figs. 7C, E).

With the strongest commercially available gradients in a 70 cm bore system, MAGNETOM Vida is perfectly balancing the needs of neuro imaging research and high-end body imaging. By combining this gradient performance with SliceAdjust, a new technique for distortion-free whole-body DWI (Fig. 9), accurate information is delivered to aid in treatment planning, e.g. in patients with multiple myeloma.

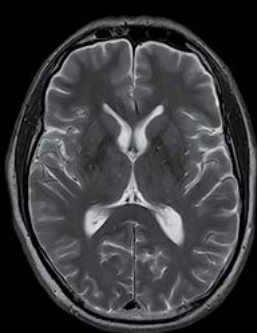
¹MR scanning has not been established as safe for imaging fetuses and infants less than two years of age. The responsible physician must evaluate the benefits of the MR examination compared to those of other imaging procedures.



1A

T2w Quiet TSE DarkFluid tra

Head/Neck 20 with 18° tilt,
TA 1:39 min x 2, TI 2500 ms,
TR 9000 ms, TE 84 ms,
FOV 199 x 220, matrix 203 x 320,
SL 5 mm



1B

T2w Quiet TSE tra

Head/Neck 20 with 18° tilt,
TA 0:45 min, TR 6400 ms,
TE 96 ms, PAT factor 3,
FOV 220 x 220, matrix 640 x 640
interpolated, SL 5 mm



1C

T2w TSE cor

Head/Neck 64, TA 3:49 min,
TR 6200 ms, TE 89 ms,
FOV 220 x 220, matrix 288 x 384,
SL 4 mm



1D

Multi-directional diffusion-weighted EPI

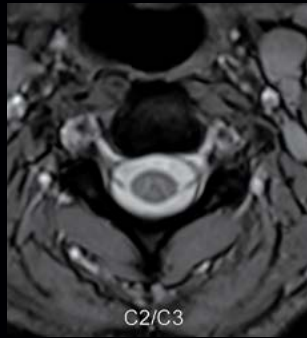
64 directions, Head/Neck 64,
TA 15:45 min, TR 4500 ms,
TE 76 ms, FOV 220 x 220,
matrix 109 x 128, 54 slices, SMS: s3



2A

T2w TSE sag with CoilShim

Head/Neck 20, TA 1:34 min x 2,
 TR 3500 ms, TE 92 ms,
 FOV 220 x 220, matrix 256 x 320,
 SL 3 mm



2B

T2w MEDIC tra

C-spine, TA 1:41 min x 2,
 TR 373 ms, TE 12 ms,
 FOV 180 x 180, matrix 436 x 512
 interpolated, SL 3 mm



4A

T1w TSE cor

Ultra Flex coil small,
 TA 1:57 min, TR 809 ms,
 TE 13 ms, FOV 120 x 120,
 matrix 358 x 512, SL 2.5 mm



4B

PDw TSE sag

Ultra Flex coil small, TA 2:20 min,
 TR 3420 ms, TE 36 ms,
 PAT factor 2, FOV 120 x 120,
 matrix 448 x 448, SL 2.5 mm



3A

T2w TSE sag



3B

**Spine Dot Engine
 AutoLabeling**



5A

T2w TSE tra

Ultra Flex coil large,
 TA 2:06 min, TR 4690 ms,
 TE 76 ms, FOV 140 x 140,
 matrix 384 x 512, SL 3 mm



5B

PDw TSE fatsat sag

Ultra Flex coil large,
 TA 3:45 min, TR 3260 ms,
 TE 33 ms, FOV 140 x 140,
 matrix 307 x 384, SL 3 mm



6A

PDw TSE Dixon cor

Body 18, Spine coil 72,
 TA 2:01 min x 2,
 TR 2700 ms, TE 37 ms,
 FOV 309 x 550,
 matrix 351 x 832, SL 3 mm



6B

PDw TSE STIR cor

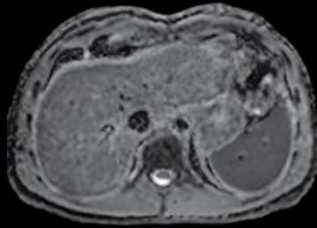
Body 18, Spine coil 72,
 TA 3:14 min, TI 220 ms,
 TR 3670 ms, TE 31 ms,
 FOV 309 x 550,
 matrix 297 x 704, SL 3 mm



6C

T1w TSE cor

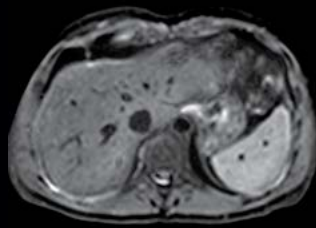
Body 18, Spine coil 72,
 TA 2:02 min x 2,
 TR 793 ms, TE 11 ms,
 FOV 241 x 550,
 matrix 274 x 896, SL 3 mm



7A

ADC map EPI diffusion with respiratory sensor

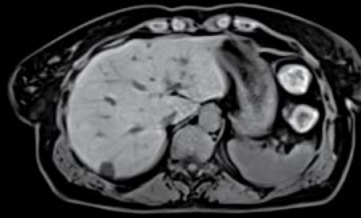
Body 18, Spine 72, TA 41 sec,
TR 2000 ms, TE 44 ms,
FOV 306 x 280, matrix 108 x 134,
SL 5 mm



7B

Trace-weighted EPI diffusion with respiratory sensor

Body 18, Spine 72, TA 41 sec,
TR 2000 ms, TE 44 ms,
FOV 306 x 280, matrix 108 x 134,
SL 5 mm



7C

T1w GRASP-VIBE fat sat tra

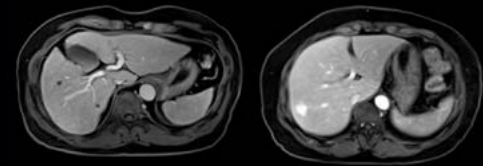
Body 18, Spine 72, TA 8 sec,
TR 3.5 ms, TE 1.3 ms,
FOV 355 x 355, matrix 256 x 256,
SL 2.5 mm



7D

T2w HASTE cor triggered

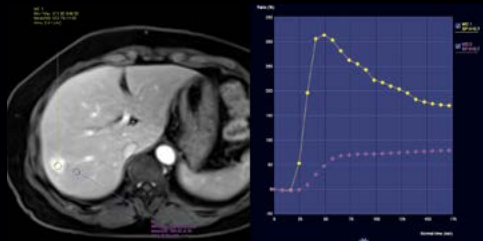
Body 18, Spine 72, TA 39 sec,
TR 2000 ms, TE 85 ms,
FOV 400 x 400, matrix 307p x 384,
SL 5 / 1 mm



7E

T1w GRASP-VIBE fat sat tra

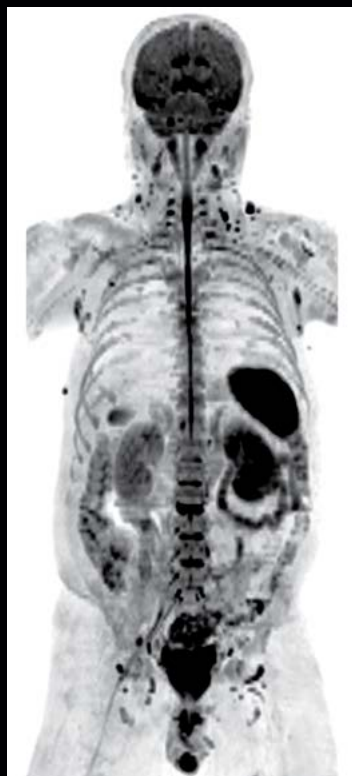
Body 18, Spine 72, series 22,
TA 8.1 sec, TR 3.5 ms, TE 1.5 ms,
FOV 450, matrix 256 x 256,
SL 3 interpolated



8

Compressed Sensing Cardiac Cine TrueFISP 5 shot sax

Body 18, Spine 32, TA 5 sec,
TR 12 ms, TE 1.3 ms, FOV 360 x 294,
matrix 189 x 240, SL 8 mm



9A

Whole-body DWI b-value 800 MIP cor



9B

Whole-body T2w TIRM cor



9C

Whole-body VIBE Dixon water cor

BioMatrix Tuners: CoilShim

Miriam R. Keil, Ph.D.; Jörg Rothard; Carmel Hayes, Ph.D.

Siemens Healthineers, Erlangen, Germany

A cervical spine or neck MRI can provide valuable diagnostic information for a wide range of different conditions. In particular, MRI's soft tissue contrast helps to detect and monitor a variety of pathologies, misalignments or injuries. It can be useful in evaluating symptoms such as pain, foreign body sensations, numbness, tingling or weakness in the arms, shoulder or neck area and can assist in detecting certain chronic diseases of the nervous system. It is also used in tumor diagnosis and in the assessment of bleeding, swelling, infections, or inflammatory conditions in the vertebrae or surrounding tissues.

In many patients, MR image quality in the neck or cervical spine region might be degraded by B_0 field distortions. These typically arise from tissue interfaces with different susceptibilities in this region, for example in the vicinity of the lung, between vertebrae, fluid-filled cavities, as well as from the body contour itself in the shoulders and neck area (Fig. 1). The low field homogeneity poses a challenge to MR imaging in this region and is often the source of image quality issues. Examples include insufficient fat saturation, spatial variations in the signal strength along the vertebrae, as well as regions showing complete signal loss.

With MAGNETOM Vida a new technology platform, BioMatrix, is introduced, which combines the ability to adapt to the individual patient's biovariability and the established Tim integrated matrix coil technology. This, in particular, allows to substantially improve image quality in the neck

area by utilizing CoilShim. CoilShim is one of the new BioMatrix technologies which allows for correction of patient-induced B_0 field inhomogeneities using dedicated shimming channels integrated into the Head/Neck coil.

Two new Head/Neck coils support CoilShim: the BioMatrix Head/Neck 20 TCS (Tilttable, CoilShim) and the BioMatrix 64 CS (CoilShim). A first step in the compensation of patient-induced B_0 field inhomogeneities is the identification of the origin of these variations. Experiments indicate that there are two major sources of B_0 field inhomogeneities in head and neck MRI. These are the patients' shoulders on the one hand and the B_0 field distortion due to the neck on the other hand. The inhomogeneity pattern originates from the geometric shape of the human body in the head and neck area and the resulting difference in susceptibilities. Figure 1 shows a typical B_0 field inhomogeneity 'map' of the head and neck region. The map was generated from a principal component analysis performed on datasets from 19 volunteer scans. The analysis showed that only the first main component contains significant information. This suggests that the inhomogeneity pattern is likely to be the same for different body shapes and sizes and that only the magnitude of the inhomogeneity varies. To correct for B_0 field inhomogeneities in the shoulder and neck region, each of the two head and neck coils is equipped with two CoilShim channels (Fig. 2). The CoilShim channels are located in the posterior part of the Head/Neck coils,

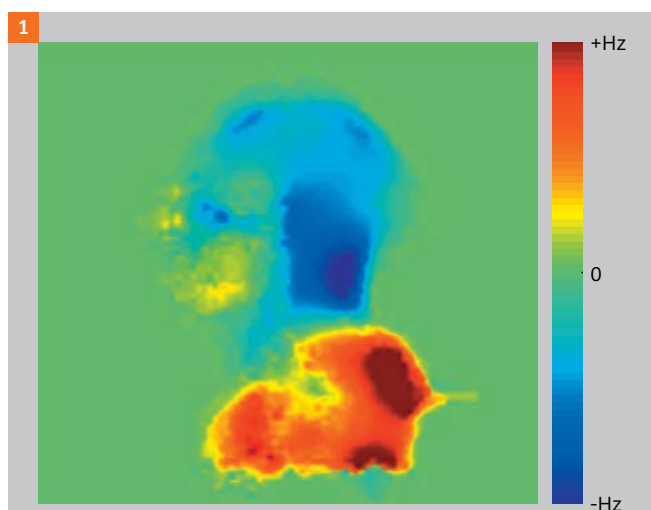


Figure 1: Typical B_0 field distortion pattern as seen in the sagittal orientation.



Figure 2: BioMatrix Head/Neck 20 TCS coil design and the location of the CoilShim elements in the BioMatrix Head/Neck 20 TCS coil.

allowing the CoilShim technology to be used even when the anterior part of the Head/Neck coils are detached. The magnitude of the B_0 field generated by each CoilShim channel can be adjusted independently with very fine resolution. This allows for best possible B_0 homogenization for each individual patient.

In order to ensure both adequate image quality and patient safety with the new Head/Neck coils with integrated CoilShim, special measures have been taken. These measures ensure decoupling of the CoilShim elements during the transmit phase and decoupling from the gradient system during the transmit and receive phase of the MR acquisition.

Applications

The usage of CoilShim requires no dedicated patient preparation: the patient can be positioned within the Biomatrix Head/Neck coil¹ as with any other head coil. When using the 20-channel TCS coil, the tilt angle may be adapted to the patients' needs, thereby providing increased patient comfort. Tilting the coil does not interfere with the CoilShim functionality but CoilShim may improve image quality degradations resulting from tilting.

CoilShim can be used with all clinical head and neck sequences and protocols, provided that the BioMatrix Head/Neck coil is plugged and active. "CoilShim" is turned on in the user interface by switching the respective parameter, which can be found on the tabcard "System", sub tab "Adjustments" from "Off" to "Auto". The actual enabling of CoilShim technology itself is therefore controlled automatically, depending on the slice geometry and the protocol parameters.

Results

The physical effect of the CoilShim feature on the B_0 field is illustrated in Figure 3, acquired in a healthy volunteer. The images compare B_0 field maps obtained using clinical state-of-the-art standard shimming with those which result from the usage of CoilShim technology.

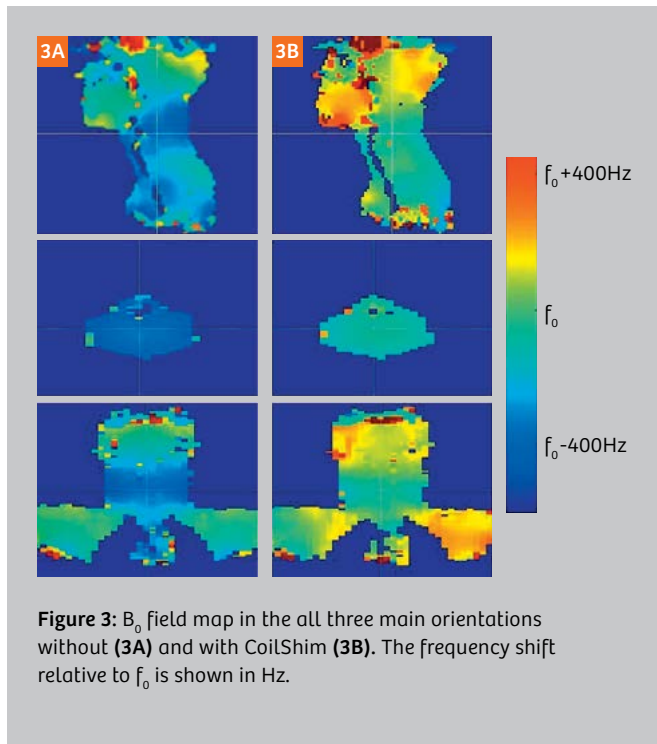


Figure 3: B_0 field map in the all three main orientations without (3A) and with CoilShim (3B). The frequency shift relative to f_0 is shown in Hz.

The images show relative resonance frequency shifts in three orthogonal slice orientations. Once again, the two dominant sources of field inhomogeneity in the shoulder and in the neck area can be observed. In this example the frequency shift in the shoulder region is about 400 Hz and the frequency shift in the neck area is about -200 Hz. Given that the frequency shift between fat and water is 430 Hz at 3T, non-uniform fat saturation can be expected in such cases.

To further illustrate the impact of CoilShim on the quality of the shimmed region of interest, Figure 4 shows the frequency distribution of all voxels within the adjustment volume both with and without CoilShim. The spectrum of the frequencies within the adjustment volume is narrowed on applying CoilShim.

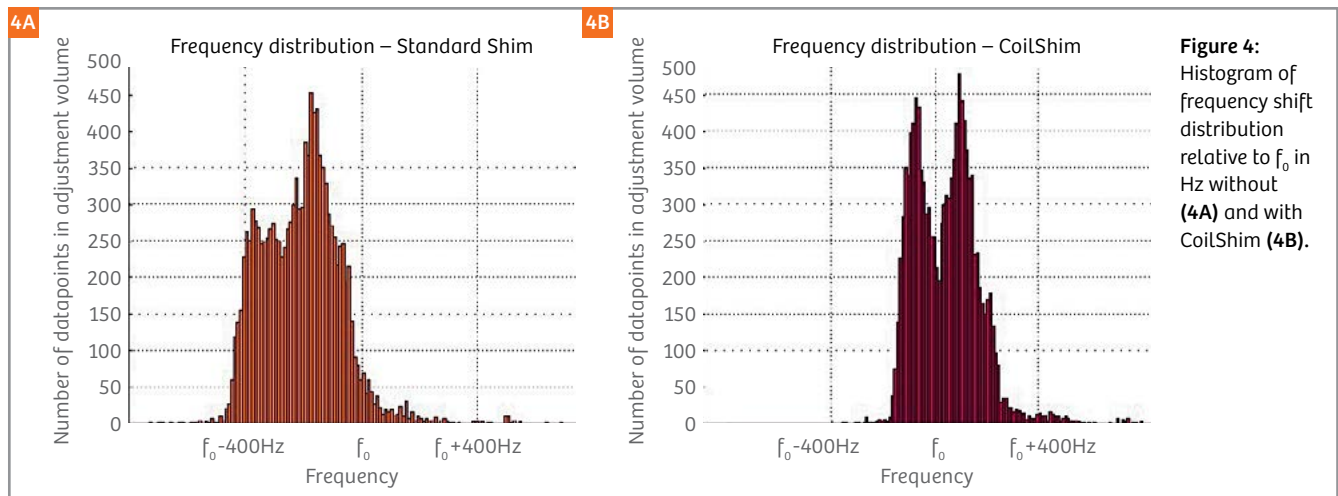


Figure 4: Histogram of frequency shift distribution relative to f_0 in Hz without (4A) and with CoilShim (4B).

The improved field homogeneity is beneficial for all MR imaging studies in the head and neck. Applications which require a highly homogenous field, for example fat saturated or SPAIR images, or EPI-based imaging, benefit in particular from local shimming. Figures 5 and 6 show typical image examples obtained in several volunteers of different

physical constitution. Figure 5 shows T1-weighted, fat saturated TSE images of the c-spine, Figure 6 illustrates the benefits of CoilShim in T2-weighted TSE images obtained with SPAIR preparation pulses. An axial T2-weighted BLADE image with SPAIR preparation pulses is shown in Figure 7. All examples show that more homogeneous fat saturation



Figure 5: T1-weighted TSE images with fat saturation in five different volunteers. Using CoilShim (lower row) improved the fat saturation not only within the vertebrae but also in the posterior areas. The contrast between vertebrae and disk is also improved.

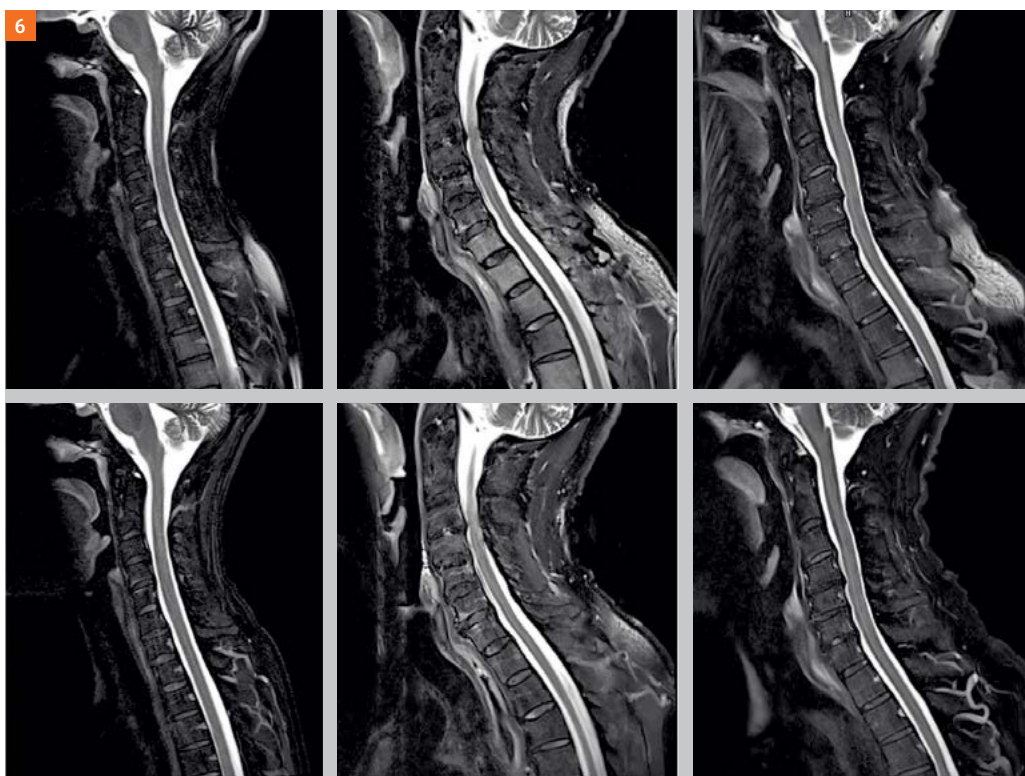


Figure 6: T2-weighted TSE images with SPAIR fat saturation in three different volunteers. Note the intensity gradient within the vertebrae without CoilShim (upper row). The image with active CoilShim on the right shows better homogeneity within the vertebrae and less contribution of unsaturated fatty tissue.

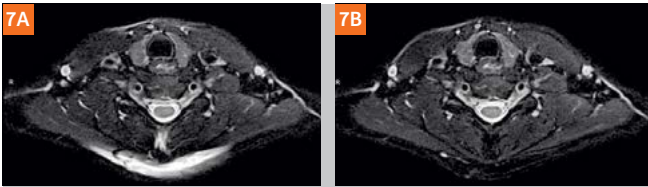


Figure 7: T2-weighted BLADE images with SPAIR fat saturation. The same imaging protocol was used without (7A) and with (7B) CoilShim. The fat saturation is more homogeneous when CoilShim is active.

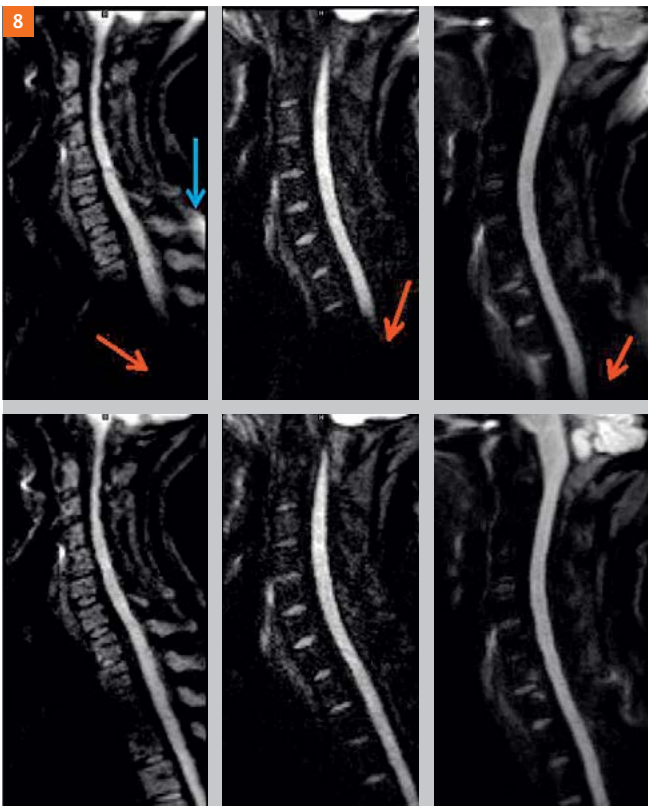


Figure 8: RESOLVE images of the c-spine with $b=600 \text{ mm/s}^2$ in three volunteers. Note the lack of signal (red arrow) in the spinal canal when measured without CoilShim (upper row). Fat saturation is also more consistent (blue arrow).

can be achieved with CoilShim. This in turn facilitates better lesion differentiation, in particular in the lower vertebrae.

Figure 8 shows RESOLVE diffusion-weighted images with a b -value of 600 mm/s^2 with and without CoilShim. Until now the display of the entire spinal canal was challenging, with CoilShim it becomes feasible to follow the spinal canal over the whole field-of-view.

Imaging methods which employ radial trajectories, for example the StarVIBE sequence, or methods such as TrueFISP, which demand a high field uniformity, also benefit from CoilShim technology and produce sharper or more

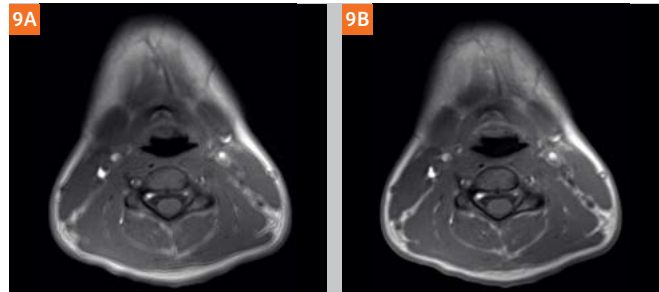


Figure 9: Radial sequences like the StarVIBE also benefit from higher field homogeneity. (9A) was measured without CoilShim, (9B) with active CoilShim. Note the increased image sharpness with CoilShim.

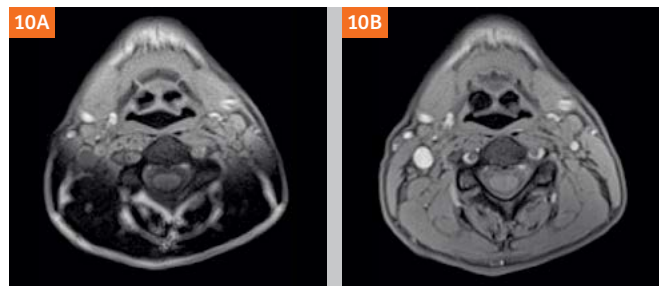


Figure 10: T1-weighted StarVibe images acquired in the neck. CoilShim (10B), can correct the field distortions which caused a shift in the frequency spectrum, inducing water saturation and corrupting image quality.

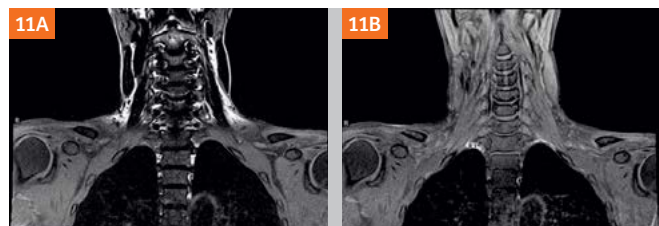


Figure 11: In rare cases, the field inhomogeneities at the border between neck and thorax are so severe, that the frequency is shifted. In these extreme examples, CoilShim (11B) also helps to mitigate the effects.

homogeneous images. Figure 9 compares StarVIBE images obtained with and without CoilShim. Less homogeneous B_0 fields broaden the frequency spectra, leading to a shift in the readout direction. Since radial sequences sample k -space not in one, but in various directions, any off-resonance dephasing shift effect is propagated into a different direction, leading to blurred images. Larger variations in B_0 homogeneity can cause frequency shifts, which in turn lead to a degradation in image contrast, as shown in Figure 10 for a StarVIBE, and in Figure 11 for a TSE acquisition. Such issues can be avoided when using CoilShim.



Figure 12: Combining CoilShim with SliceAdjust leads to significant image quality improvements in diffusion-weighted imaging. The same slice is compared without CoilShim and SliceAdjust (upper row) and with active CoilShim and SliceAdjust (lower row). From left to right: $b=50 \text{ s/mm}^2$, $b=800 \text{ s/mm}^2$, ADC.

In combination with SliceAdjust, CoilShim technology allows for robust diffusion-weighted imaging (DWI) in the neck area. In the past, DWI imaging of the c-spine or neck soft tissue was challenged by distortions, low signal intensity and artefacts. On enabling the BioMatrix Tuners, the image quality can be improved significantly. Figure 12 illustrates the advantages of CoilShim and SliceAdjust when activated in a DWI image of the neck.

Practical tips

CoilShim is designed to optimize, in particular, the field homogeneity in the cervical spine. Therefore, it works best when imaging the cervical spine, especially in sagittal slice orientations. However, the whole neck area benefits when using CoilShim, although there are some physical limitations. First of all, as the CoilShim elements are located for safety reasons in the lower part of the Head/Neck coil, the scope of the feature is regionally restricted. For this reason, a drop in B_0 field homogeneity in the vicinity of the anterior part of the neck or the chin area may be observed. This effect may be manifested, as shown in Figure 13 for example, by inhomogeneous fat saturation in the chin area due to the regional limitations of the CoilShim field. The same applies to the shoulders, since the CoilShim elements cannot cover the entire shoulder region. This is shown in Figure 14. Another occasionally-observed effect is a frequency change in the t-spine next to the lung, seen usually in coronal images. As CoilShim optimizes the c-spine and cannot reach the vertebrae of the t-spine, the B_0 field

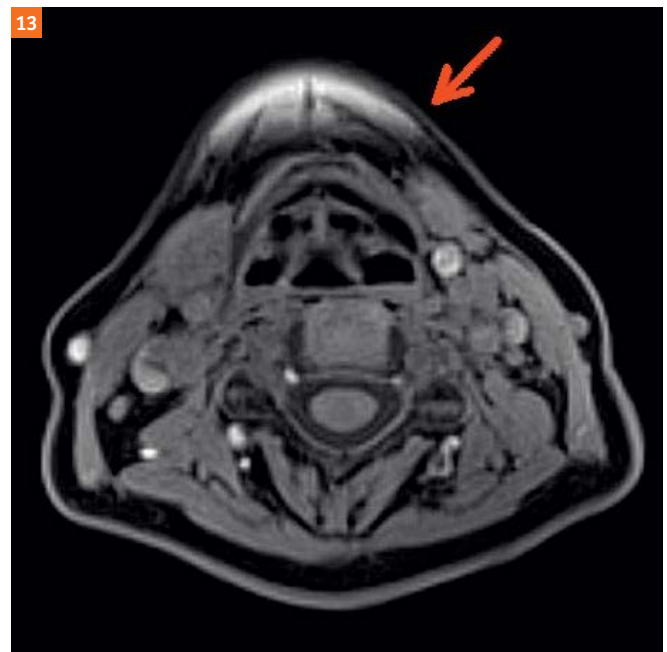


Figure 13: Anterior regions like the chin cannot be reached by CoilShim, which is located in the posterior neck coil region. Typically, in such cases, small regions with insufficient fat saturation are observed.

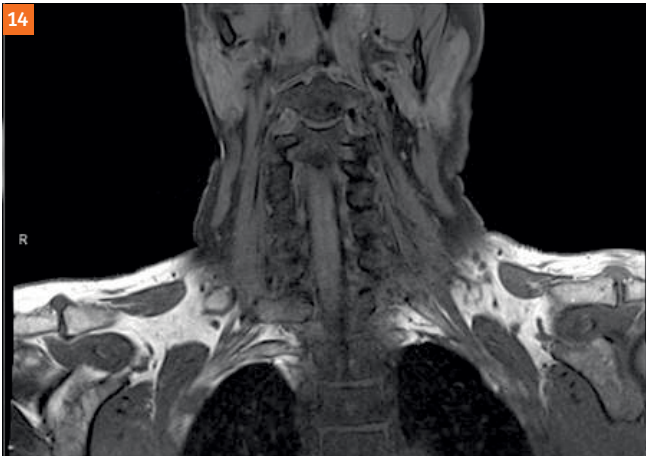


Figure 14: The local effectiveness of the CoilShim elements can lead to less efficient fat saturation in the lateral shoulder area.

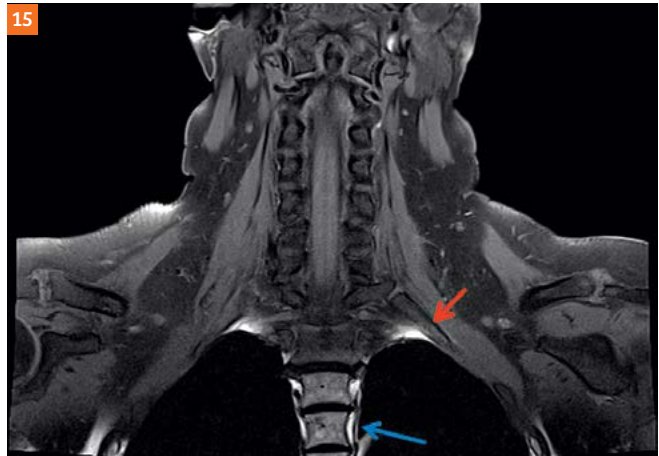


Figure 15: Typical lung-tip artefact (red arrow) and water saturation (blue arrow) in the t-spine. Note the homogeneous fat saturation in the neck/shoulder area.

is dominated by the lung, which might lead to lower field homogeneity with degradations in image quality in the t-spine as shown in Figure 15. The same image also shows the so called lung-tip artefact, which originates from local field distortions, leading to a less efficient fat saturation in a small area around the lung apex.

Summary

CoilShim addresses field disturbances within the head and neck region by local, patient-adapted shim currents. This helps to homogenize the static magnetic field in this region. Thereby the image quality can be improved. Typical benefits include more homogeneous fat saturation, less blurring in radial sequences and more signal with diffusion weighted imaging. Since CoilShim is based on new hardware and transmit pathways, it is currently only available with the BioMatrix Head/Neck coils. Nonetheless, this new technology might also be useful to improve B_0 homogeneity in other body regions in the future.

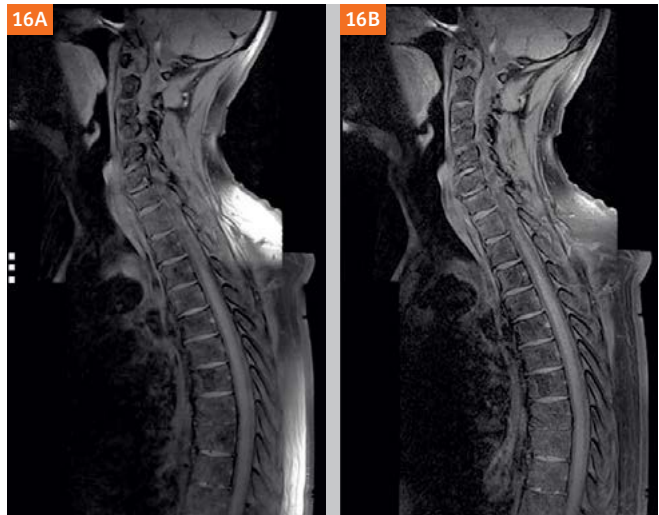


Figure 16: Composing for whole-spine representations also benefits from CoilShim (16B).

Contact

Miriam Keil
Siemens Healthcare GmbH
HC DI MR R&D SYS APPL
Post Box 91050
91050 Erlangen
Germany
Phone: +49 (9131) 84-4671
miriam.keil@siemens-healthineers.com



Miriam R. Keil



Jörg Rothard



Carmel Hayes

Slice Specific Shimming Improves the Image Quality of Whole-Body Diffusion-Weighted Examinations at 3T

Zhang Haibo¹; Xue Huadan²; Alto Stemmer³; Liu Hui⁴; Stephan Kannengiesser³; Berthold Kiefer³; Jin Zhengyu²

¹ Department of Radiology, China-Japan Friendship Hospital, Beijing, China

² Department of Radiology, Peking Union Medical College Hospital, Peking Union Medical College and Chinese Academy of Medical Sciences, Beijing, China

³ MR Application-Predevelopment, Siemens Healthineers, Erlangen, Germany

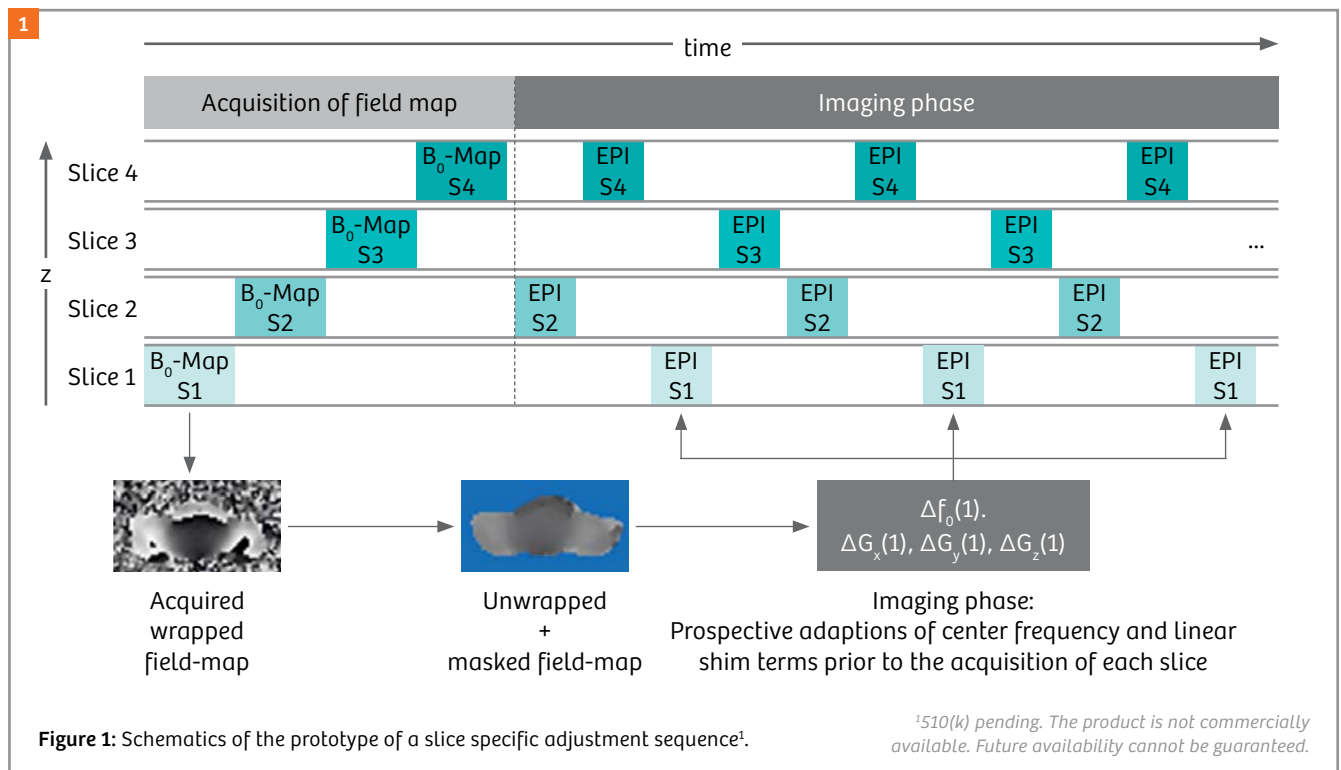
⁴ MR Collaboration, Siemens Healthineers, Shanghai, China

Current whole-body diffusion-weighted imaging

Whole-body diffusion-weighted imaging (WBDWI) is considered a powerful clinical tool in the detection, characterization, and treatment-response monitoring of tumors [1, 2]. It has been increasingly used in the evaluation of multiple myeloma, lymphoma, and skeletal metastases [3–8]. Being a measure of the microscopic water motion, WBDWI provides a quantitative way of evaluating the tissue cellularity using the apparent diffusion coefficient (ADC). For example, whole-body magnetic resonance imaging including WBDWI is sensitive to multiple myeloma, especially in the case of diffuse bone marrow infiltration [9]. The combination of WBDWI with Fluorodeoxyglucose Positron Emission Tomography (FDG-PET) may provide a

multi-parametric assessment of tumors due to complementary imaging principles, where diffusion-weighted imaging (DWI) evaluates the tumor cellularity and the FDG-PET assesses the tumor metabolism [10].

At present it is challenging to meet the clinical demands for image quality with WBDWI at 3 Tesla. The signal-to-noise ratio (SNR) is increased at 3T, but it is still a challenge to perform WBDWI due to the drawback of single-shot echo planar imaging (EPI) acquisition and the stronger susceptibility effects, which lead to stronger geometric distortions and poor fat-suppression performance in specific body regions such as the neck. The distortions Δd in EPI are proportional to the physical field-of-view (FOV) in the phase-encoding direction (FOV_{PE}), the echo spacing Δt_{PE} and the local off-resonance ΔB_0 ($\Delta d \sim FOV_{PE} \times \Delta t_{PE} \times \Delta B_0$).



Recent technical developments in DWI acquisition such as readout segmented EPI [11, 12], other multi-shot [13] and zoomed techniques [14, 15] have shown improvements with less geometric distortion and higher image quality from the perspective of reducing Δt_{PE} or FOV_{PE} . However, the above techniques are not clinically feasible for whole-body imaging because of longer acquisition time, FOV restrictions, or sensitivity to motion.

Slice specific adjustment

Several past studies have shown the feasibility of reduced susceptibility artifact by dynamically updating optimized shim settings for each individual slice in a multi-slice acquisition [16]. Another study using slice-dependent adjustment has also shown improved image quality in 3T breast DWI [17]. However, its advantage to WBDWI is still unknown. The approach described here is to use slice specific adjustments for WBDWI, where a 2D multi-echo gradient echo (GRE) sequence preceding the WBDWI EPI scan is used to acquire a B_0 -map for each imaging slice. From the B_0 -map an optimal center frequency and linear shim terms are determined for each imaging slice. Center frequency and gradient offsets are then updated before the acquisition of each EPI imaging slice in real time. In a recent study, its performance was evaluated, comparing slice specific adjustment to a conventional pre-scan based shimming technique (3D Shim) [18].

For the 3D Shim protocol, one set of shim terms up to 2nd order is used for the entire slice stack of each patient table position, and the acquisition of the field map is included in the automatic scanner adjustment, which takes approximately 33 seconds per station (35 slices per station). Additionally, a single center frequency is determined in a separate frequency adjustment. Center frequency and shim currents are set once prior to the EPI scan.

For the slice specific adjustment protocol, the patient-specific 3D Shim procedure in the automatic scanner adjustment is disabled. The acquisition of the field map is integrated into the single-shot DWI EPI sequence. This prototype sequence first acquires 2D multi-gradient-echo images for each imaging slice with its FOV and orientation adapted from the respective imaging slice. The echo-time difference of the first and last echo is chosen such that fat and water are in-phase. Then a phase difference image is calculated from these two echoes. The remaining processing of the field map data is done in 3D and comprised phase unwrapping, background masking and a calibration to avoid global 2π offsets after unwrapping. For the dynamic shimming, a 2D plane is fitted to each field map slice to determine the center frequency and gradient offsets (1st order shim terms). Center frequency and gradient offsets are then updated before the acquisition of each EPI imaging slice in real time (Fig. 1). The time for the acquisition of the field map is approximately 540 ms per slice, or 19 s for a 35 slices station. Processing time of the field map is negligible.

Clinical evaluation

The evaluation of the slice specific adjustment technique for WBDWI in comparison to the conventional 3D Shim was performed at Peking Union Medical College Hospital. The slice specific adjustment and the 3D Shim WBDWI acquisitions with the exact same scan parameters were performed sequentially, and the impact of different shimming techniques on the image quality and detectability of conspicuous lesions were quantitatively analyzed and evaluated. Body-region-dependent signal-to-noise ratio (SNR), body-region-dependent shimming parameters, image quality, and the number of suspicious lesions were compared in 2 volunteers and 29 patients with suspected plasma-disorder. The results were as follows:

1. SNR

Two volunteers' position-dependent SNR ratio of slice specific adjustment over 3D Shim showed a significant SNR improvement with slice specific adjustment in the neck region, and a comparable SNR in other body regions. For the neck region, none of the 29 patients showed obvious signal loss with slice specific adjustment, while 25 patients showed partial to complete signal loss with 3D Shim scanning (Fig. 2).

2. Position-dependent slice specific adjustment parameters

The position-dependent slice specific adjustment parameters, center frequency shift, and linear frequency shift in phase-encoding direction, deviated significantly from the corresponding values of the 3D Shim settings only in the neck region, while they were comparable in the other body regions.

3. Image quality

Spatial displacement of DWI images was quantified by comparison with reformatted T2 SPACE images. This displacement was evaluated from cervical to coccyx vertebrae, excluding the neck region with signal loss (Figs. 2, 3). The mean absolute spatial displacement of the spine was 3.89 mm for slice specific adjustment and 7.21 mm for 3D Shim, respectively. The slice specific adjustment technique showed a significantly better illustration of the body shape than 3D Shim WBDWI.

4. Lesion detection assessment

Visual inspection of slice specific adjustment and 3D Shim DWI images side by side showed that the same lesions could be observed with both techniques in the thorax, abdomen and pelvis regions, while 24 of 72 lesions visible in slice specific adjustment DWI images of the neck region were not visible in 3D Shim DWI images; all lesions observed in 3D Shim DWI were also visible in slice specific adjustment DWI images.

Discussion

Signal loss is very common in the neck region of conventional 3D Shim WBDWI because there the B_0 varies rapidly along the head-foot direction caused by the sudden change of the

body shape. Especially when a body station covers the neck and part of the shoulder region, the 3D Shim adjustment may be insufficient since one single setting of resonance frequency and shim terms is not able to homogenize the B_0 field in the whole volume. In this study, the neck region showed a larger variation of center frequency shift and linear frequency shift in the phase-encoding direction than other body regions, and at the same time the lowest image quality of 3D Shim images, which supports this hypothesis. By applying a slice-based individual center frequency and gradient offset setting, the slice specific adjustment technique produced improved SNR and reliable image quality in the neck region and therefore outperforms 3D Shim. In other body regions such as thorax, abdomen and pelvis, there were no significant differences between slice specific adjustment and 3D Shim WBDWI for lesions and muscle.

WBDWI provides a global assessment of whole-body tumor burden by visually assessing the signal intensity distribution on maximum intensity projections (MIPs) from high-b-value images. Practically, the whole-body images are acquired with multiple patient table positions, and are then composed to show the whole-body view (Fig. 3). Therefore, the signal homogeneity across different body parts is quite important, and lesions spanning images from adjacent patient table positions might be missed or misidentified as a result of large signal differences between these images. The image quality evaluation showed that the slice specific adjustment technique produced a smoother signal transition between

adjacent patient table positions than the 3D Shim technique.

It is possible to further reduce the remaining distortions significantly with a recent extension of the slice specific adjustment prototype sequence as described in [19]. The modification combines the prospective slice-specific center-frequency adjustment and 1st order shimming with retrospective distortion correction based on the field-map method [20]. The field-map method uses a measured field-map to undo the distortion on a pixel-wise scale during post-processing. In the combined method, the field-map needed for the distortion correction is not re-measured after center frequency adjustment and shimming but calculated from the field-map measured at the beginning and the known frequency and shim settings. It therefore does not prolong the acquisition time. It is a matter of further evaluation to enroll new patients to test the slice specific adjustment method together with retrospective distortion correction.

Short TI Inversion Recovery (STIR) fat suppression, which was used here, leads to lower SNR compared with chemical-shift-based fat suppression methods since water signal which is also inverted by the inversion pulse is not fully recovered at excitation time. Chemical shift based fat suppression techniques, however, are very sensitive to B_0 inhomogeneity [21, 22], so that the image quality can be degraded by fat ghosting or water suppression. As slice specific adjustment helps to significantly reduce the B_0 inhomogeneity, chemical shift based fat suppression

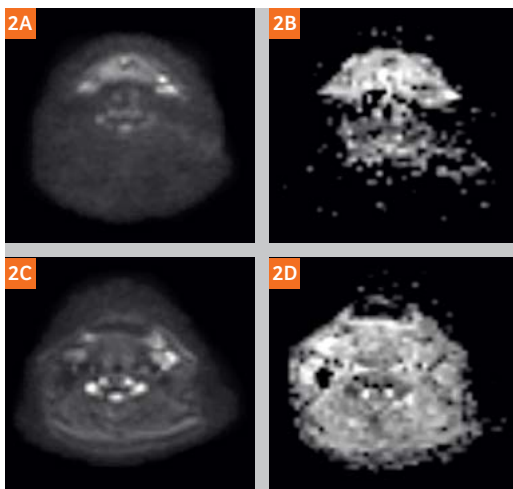
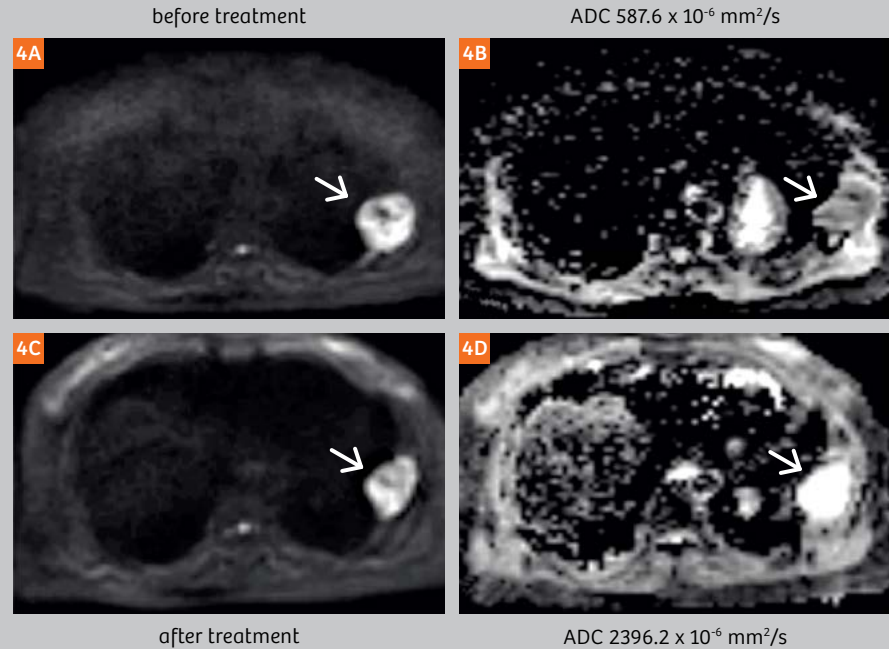


Figure 2: Transversal view of the selected single slice of the neck of the same patient: **(2A)** 3D Shim DWI ($b = 800 \text{ s/mm}^2$), **(2B)** ADC map of 3D Shim DWI ($b = 800 \text{ s/mm}^2$), **(2C)** slice specific adjustment DWI ($b = 800 \text{ s/mm}^2$) and **(2D)** ADC map of slice specific adjustment DWI ($b = 800 \text{ s/mm}^2$). **2A, B** showed massive signal loss in the neck region of 3D Shim DWI, however slice specific adjustment technique improved the image quality of the neck region obviously.



Figure 3: Maximum intensity projections (MIPs) with inverted grayscale from high-b-value WBDWI images. **(3A, B)** 3D Shim WBDWI images. However, in the neck region a strong image quality deterioration can be observed. **(3C, D)** Slice specific adjustment WBDWI images. Compared with 3D Shim WBDWI, slice specific adjustment WBDWI showed artifact-free images.

Figure 4: 57-year-old female patient with multiple myeloma on the left chest wall (arrows). (4A, B) show a lesion with high signal on DWI ($b = 800 \text{ s/mm}^2$) image and low ADC value ($587.6 \times 10^{-6} \text{ mm}^2/\text{s}$) before treatment. (4C, D) show that the lesion still existed five months later after treatment, but ADC value was much higher than before. The change in ADC corresponds with the clinical results.



techniques might provide an efficient fat suppression from head to toe. Chemical shift based fat suppression techniques like Spectral Adiabatic Inversion Recovery (SPAIR) are not compatible with slice specific adjustment as they exploit non-selective RF-pulses. Instead, slice selective water excitation could be used with slice specific adjustment. The inherently higher SNR of water excitation may allow reducing the number of averages and hence the total acquisition time, and it merits evaluation in a clinical setting.

Conclusion

The slice specific adjustment technique is an effective method to reduce the negative impact of susceptibility effects on whole-body diffusion-weighted imaging at 3T, as supported by the apparent improvement in image quality, as well as improved SNR in the neck region. Compared with the 3D Shim technique, slice specific adjustment showed improved performance in detecting suspicious lesions in the neck region. The slice specific adjustment technique has entered the clinical arena, improving WBDWI. Slice specific adjustment and its future refinements may further improve the accuracy of lesion assessment and monitoring treatment response (Fig. 4).

References

- ¹Padhani AR, Liu G, Koh DM, et al. Diffusion-weighted magnetic resonance imaging as a cancer biomarker: consensus and recommendations. *Neoplasia* 2009;11(2):102–125.
- ²Padhani AR, Koh DM, Collins DJ. Whole-body diffusion-weighted MR imaging in cancer: current status and research directions. *Radiology* 2011;261(3):700–718.
- ³Attariwala R, Picker W. Whole body MRI: improved lesion detection and characterization with diffusion weighted techniques. *J MagnReson Imaging* 2013;38(2):253–268.

⁴Petralia G, Padhani A, Summers P, et al. Whole-body diffusion-weighted imaging: is it all we need for detecting metastases in melanoma patients? *EurRadiol*. 2013;23(12):3466–3476.

⁵Brioli A, Morgan GJ, Durie B, Zamagni E. The utility of newer imaging techniques as predictors of clinical outcomes in multiple myeloma. *Expert RevHematol* 2014;7(1):13–16.

⁶Mayerhoefer ME, Karanikas G, Kletter K, et al. Evaluation of diffusion-weighted MRI for pretherapeutic assessment and staging of lymphoma: results of a prospective study in 140 patients. *Clin Cancer Res* 2014;20(11):2984–2993.

⁷Littooij AS, Kwee TC, Barber I, et al. Whole-body MRI for initial staging of paediatric lymphoma: prospective comparison to an FDG-PET/CT-based reference standard. *EurRadiol* 2014;24(5):1153–1165.

⁸Klenk C, Gawande R, Uslu L, et al. Ionising radiation-free whole-body MRI versus (18)F-fluorodeoxyglucose PET/CT scans for children and young adults with cancer: a prospective, non-randomised, single-centre study. *Lancet Oncol* 2014;15(3):275–285.


⁹Zamagni E, Nanni C, Patriarca F, et al. A prospective comparison of 18F-fluorodeoxyglucose positron emission tomography-computed tomography, magnetic resonance imaging and whole-body planar radiographs in the assessment of bone disease in newly diagnosed multiple myeloma. *Haematologica*.2007; 92(1):50-55.

¹⁰Schmidt H, Brendle C, Schraml C, et al. Correlation of simultaneously acquired diffusion-weighted imaging and 2-deoxy-[18F] fluoro-2-D-glucose positron emission tomography of pulmonary lesions in a dedicated whole-body magnetic resonance/positron emission tomography system. *Invest Radiol*. 2013;48(5):247-55.

¹¹Bogner W, Pinker-Domenig K, Bickel H, et al. Readout-segmented echo-planar imaging improves the diagnostic performance of diffusion-weighted MR breast examinations at 3.0 T. *Radiology* 2012;263(1):64–76.

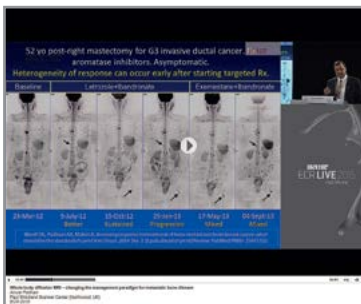
¹²Porter DA, Heidemann RM. High resolution diffusion-weighted imaging using readout-segmented echo-planar imaging, parallel imaging and a two-dimensional navigator-based reacquisition. *Magn Reson Med*. 2009;62(2):468–475.

- ¹³Chen NK, Guidon A, Chang HC, et al. A robust multi-shot scan strategy for high-resolution diffusion weighted MRI enabled by multiplexed sensitivity-encoding (MUSE). *Neuroimage* 2013;72:41–7.
- ¹⁴Riffel P, Michaely HJ, Morelli JN, et al. Zoomed EPI-DWI of the head and neck with two-dimensional, spatially-selective radiofrequency excitation pulses. *EurRadiol* 2014; 24(10):2507–12.
- ¹⁵Thierfelder KM, Scherr MK, Notohamiprodjo M, et al. Diffusion-weighted MRI of the prostate: advantages of Zoomed EPI with parallel-transmit-accelerated 2D-selective excitation imaging. *EurRadiol* 2014; 24(12):3233–41.
- ¹⁶Morrell G, Spielman D. Dynamic shimming for multi-slice magnetic resonance imaging. *MagnResonMed* 1997;38(3):477–83.
- ¹⁷Lee SK, Tan ET, Govenkar A, et al. Dynamic slice-dependent shim and center frequency update in 3 T breast diffusion weighted imaging. *MagnReson Med* 2014;71(5):1813–1818.
- ¹⁸Zhang H, Xue H, Stemmer A, et al. Integrated Shimming Improves Lesion Detection in Whole-Body Diffusion-Weighted Examinations of Patients With Plasma Disorder at 3 T. *Investigative Radiology*, 2015 [Epub ahead of print]
- ¹⁹Stemmer A and Kiefer B. Combination of integrated slice-specific dynamic shimming and pixel-wise unwarping of residual EPI distortions. *Proc. Intl. Soc. Mag. Reson. Med.* 2015; 23:3729.
- ²⁰Jezzard P and Balaban RS. Correction for geometric distortion in echo planar images from B0 field variations. *Magnetic Resonance in Medicine* 1995; 34:65–73.
- ²¹Takahara T, Imai Y, Yamashita T, et al. Diffusion weighted whole body imaging with background body signal suppression (DWIBS): technical improvement using free breathing, STIR and high resolution 3D display. *Radiat Med.* 2004;22:275–282.
- ²²Thomas C, Kwee, Taro Takahara, Reiji Ochiai, et al. Diffusion-weighted whole-body imaging with background body signal suppression (DWIBS): features and potential applications in oncology". *EurRadiol.* 2008; 18:1937–1952
- ²³Messiou C, Giles S, Collins D J, et al. Assessing response of myeloma bone disease with diffusion-weighted MRI [J]. *The British journal of radiology*, 2012, 85(1020): e1198–203.
- ²⁴Giles S L, Messiou C, Collins D J, et al. Whole-body diffusion-weighted MR imaging for assessment of treatment response in myeloma [J]. *Radiology*, 2014, 271(3): 785–94.

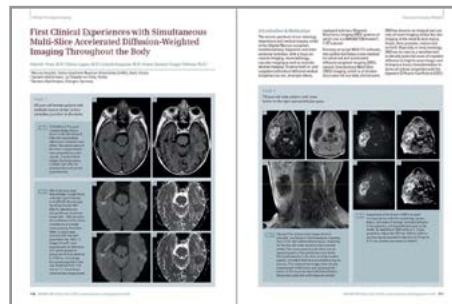
Contact	
	<p>Professor Xue Huadan, M.D. Department of Radiology Peking Union Medical College Hospital, Peking Union Medical College and Chinese Academy of Medical Sciences Shuaifuyuan 1#, Wangfujing Street, Dongcheng District Beijing, China, 100730 bjdanna95@hotmail.com</p>
	<p>Zhang Haibo, M.D. Department of Radiology Chinese-Japan Friendship Hospital Yinghuayuan East Street #2 Chaoyang District Beijing, China, 100029 zhb_hello@163.com</p>

Learn more!

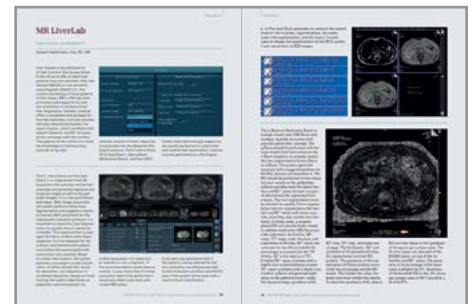
The Siemens Healthineers global MRI community offers peer-to-peer support and information. Protocols, application tips, presentations, case studies, and more are freely available via the MAGNETOM World network.



Whole-body Diffusion MRI
Anwar R. Padhani
 Paul Strickland Scanner Centre,
 Mount Vernon Hospital
 (Northwood, Middlesex, UK)



Simultaneous Multi-Slice Accelerated DWI Throughout the Whole Body
Valentin Tissot et al.
 Morvan Hospital
 (Brest, France)



How-I-do-it: MR LiverLab
Robert Sellers
 Siemens Healthineers
 (Cary, NC, USA)

Put the advantages of the MAGNETOM World to work for you!

[siemens-healthineers.us/vida-flash](https://www.siemens-healthineers.us/vida-flash)

Whole-Body Dot Engine: First Clinical Experience with Automated Chest, Abdomen and Pelvis Examinations

Cäcilia S. Reiner¹; Bernd Kuehn²; Daniel Nanz¹; Tim Finkenstädt¹; Berthold Kiefer²; Gustav Andreisek¹

¹ Institute of Diagnostic and Interventional Radiology, University Hospital Zurich, University of Zurich, Switzerland

² Oncology Application Predevelopment, Siemens Healthineers GmbH, Erlangen, Germany

Introduction

Time and cost efficiency are among the major challenges in clinical magnetic resonance imaging (MRI), mainly driven by the funding cuts in most health care systems [1]. At the same time, there is an increasing overall demand for a higher quality of MRI exams with regard to comparability, i.e. important for primary and/or follow-up studies in oncologic patients. To address these challenges, several vendors and researchers are developing automated scanner workflows for clinical MRI systems. The hypothesis is that these workflows allow a standardized and time-efficient use and provide a robust image quality with only little user interaction. The Whole-Body Dot Engine was developed

to meet these needs for multi-station MRI exams of chest, abdomen, pelvis, and even the whole body. Potential indications of multi-station body MRI exams are oncologic staging or follow-up, rheumatic disease and evaluation of myopathies.

MRI technique

The Whole-Body Dot Engine automatically detects landmarks like lung apex, lung recesses, diaphragm, liver apex, iliac bone on a fast low-resolution whole-body scout, which is acquired during moving table. Based on this scout the body regions selected for scanning, namely chest, abdomen and/or pelvis are automatically segmented (Fig. 1). With the

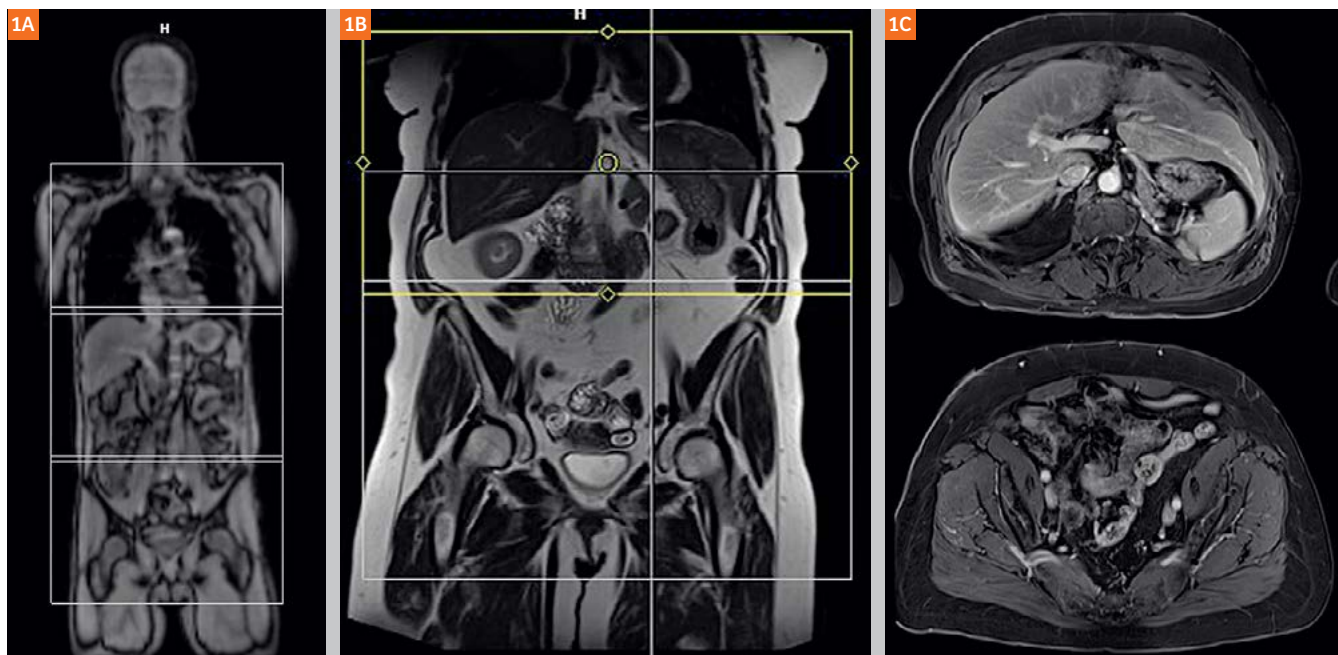


Figure 1: (1A) Fast low resolution whole-body scout with automatically segmented abdomen and pelvis for multi-station scanning. (1B) Coronal T2 single-shot turbo-spin-echo images with automatically segmented abdomen and pelvis split into two blocks for the transverse T1-weighted sequence (1C) with an acquisition time of 15 s for each. The cranio-caudal coverage per block is set to 400 mm with a fixed overlap of 2 cm between blocks and is adjusted to patient size and breath-hold capacity.

Table 1: MRI protocol.

	T2w HASTE	T2w HASTE	iShim ¹ EPI DWI	T1w VIBE Dixon without and with contrast	T1w VIBE Dixon with contrast
Scan plane	coronal	transverse	transverse	transverse	coronal
Repetition time / Echo time (ms)	1230/92	1000/60	6100/56	4.27/1.28	3.93/1.23
Flip angle (°)	160	160	90	12	12
Slice thickness (mm)	6	5	6	3	1,5
Spacing (mm)	1	1	1	0	0
Acquisition matrix	256 x 256	256 x 109	128 x 84	320 x 180	192 x 162
Acceleration, factor	GRAPPA, 3	GRAPPA, 3	GRAPPA, 2	CAIPIRINHA, 2	CAIPIRINHA, 6
Number of excitations	1	1	6 and 15	1	1
b-values (s/mm ²)	na	na	50, 800	na	na

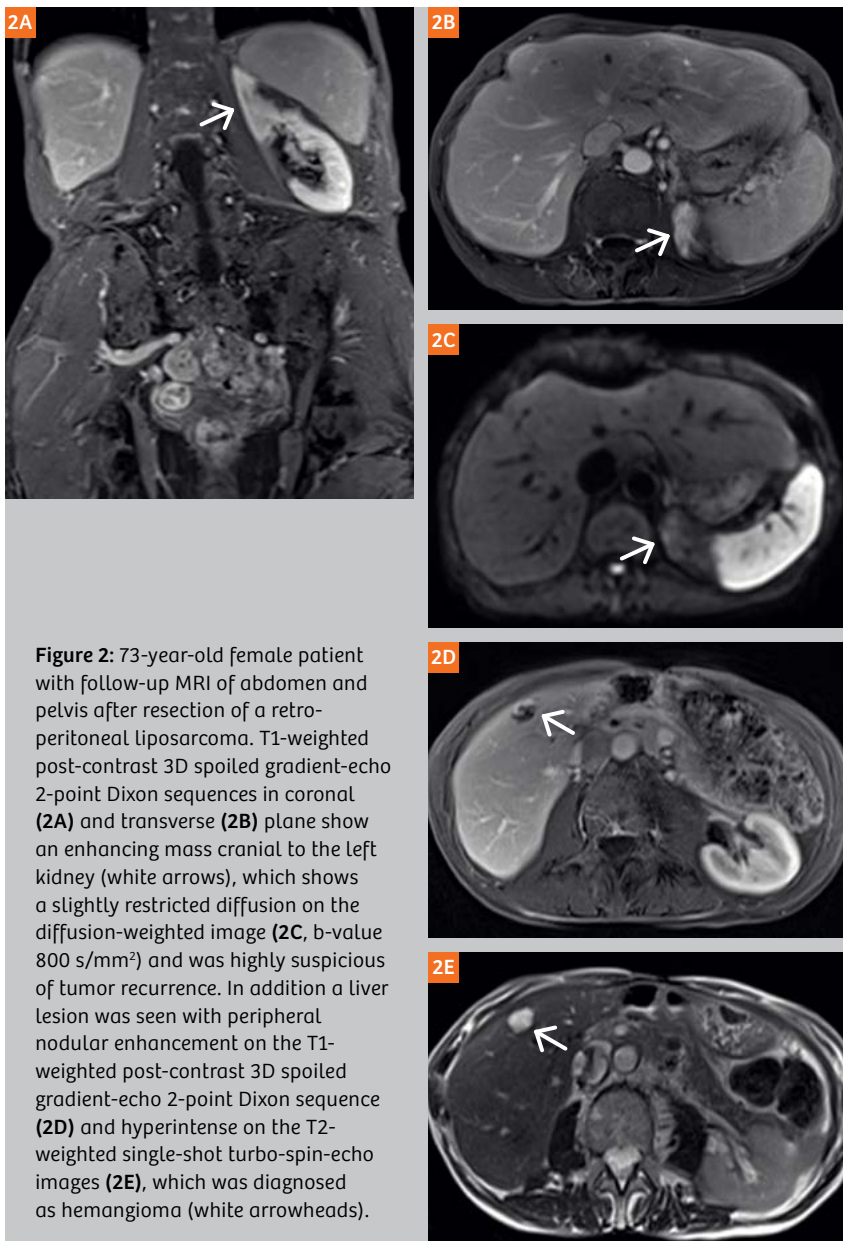


Figure 2: 73-year-old female patient with follow-up MRI of abdomen and pelvis after resection of a retro-peritoneal liposarcoma. T1-weighted post-contrast 3D spoiled gradient-echo 2-point Dixon sequences in coronal (2A) and transverse (2B) plane show an enhancing mass cranial to the left kidney (white arrows), which shows a slightly restricted diffusion on the diffusion-weighted image (2C, b-value 800 s/mm²) and was highly suspicious of tumor recurrence. In addition a liver lesion was seen with peripheral nodular enhancement on the T1-weighted post-contrast 3D spoiled gradient-echo 2-point Dixon sequence (2D) and hyperintense on the T2-weighted single-shot turbo-spin-echo images (2E), which was diagnosed as hemangioma (white arrowheads).

information of the segmentation the sequence parameters (field-of-view [FOV] and number of slices) are automatically adjusted in order to ensure proper coverage of the body regions of interest. Additionally, the Whole-Body Dot Engine uses an anticipated patient's breath-hold capacity to automatically adjust the imaging protocols in body regions where breath-hold is required to generate optimal image quality. The user can configure which parameters shall be adjusted for each protocol individually. In our protocol, base resolution was used for this purpose in 3D sequences, and number of concatenations was used in 2D sequences. We set the breath-hold capacity to 20 seconds. The protocol included a coronal and transverse T2-weighted single-shot turbo-spin-echo sequence (HASTE) acquired in breath-hold technique, transverse single-shot diffusion-weighted echo-planar imaging with slice-specific shim optimization (EPI-DWI, iShim [2]) in free-breathing, and a transverse T1-weighted pre- and post-contrast 3D spoiled gradient-echo 2-point Dixon (VIBE) sequence acquired in breath-hold technique pre- and post-contrast (delay: chest 35 s, abdomen 70 s, pelvis 90 s after injection of 0.1 mmol/kg bodyweight gadoterate meglumine, Dotarem, Guerbet) (Table). Imaging after contrast-injection was timed by using automated bolus detection. The cranio-caudal coverage per block was adjusted to 400 mm.

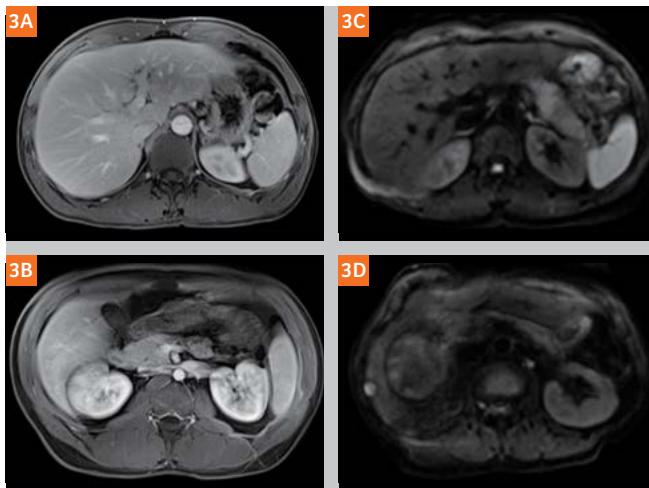


Figure 3: T1-weighted post-contrast 3D spoiled gradient-echo 2-point Dixon sequences with excellent image quality (**3A**) and with mild respiratory motion artifacts (**3B**). Single-shot diffusion-weighted echo-planar imaging sequence with slice-specific shim optimization with excellent image quality (**3C**) and with mild motion artifacts (**3D**).

We chose a rather short scan protocol without dynamic acquisitions in a focus region (e.g. liver), because we wanted a fast and straightforward protocol for general oncologic imaging comparable to computed tomography. We used this scan protocol for oncologic follow-up imaging of abdomen and pelvis or chest, abdomen, and pelvis.

Patients

20 patients (9 females, 11 males; mean age 52 years, range 21–79 years) were examined on a 3T MRI scanner (MAGNETOM Skyra, Siemens Healthineers) using the Whole-Body Dot Engine. Multi-station exams were performed on 11 patients for oncologic follow-up, in 2 for primary staging, and in 7 for tumor screening. The clinical diagnosis of these patients was: genitourinary malignancy (n=8), sarcoma (n=3), gastrointestinal malignancy (n=1), poly-posit syndromes (n=2), and chronic abdominal pain (n=6). In 18 patients abdomen and pelvis were scanned and in 2 patients chest, abdomen and pelvis. An image example is given in Figure 2. To validate whether our straightforward

protocol results in an acceptable duration of this multi-station MRI, patients scored their satisfaction with exam duration on a visual analogue scale from 0 (not acceptable, too long) to 10 (ideal exam duration).

Image quality

The scans were evaluated for overall image quality (IQ) (5 = excellent, 4 = good, 3 = moderate, 2 = poor, 1 = non-diagnostic) and artifacts (5 = no artifacts, 4 = mild artifacts, 3 = moderate artifacts, 2 = severe artifacts, 1 = non-diagnostic) on a 5-point scale by a board-certified abdominal radiologist with 8 years of experience. The image acquisition time was noted, as well as whether the coverage of the targeted body region was complete.

In all but one patient (19 of 20, 95%), the selected body regions were covered completely by the automated algorithm. An exception was the DWI, which showed markedly reduced signal in the sub-diaphragmatic part of the right liver in four patients (4 of 20, 20%), which impaired diagnostic ability of DWI in these liver parts.

The mean score for overall IQ was 4.7 ± 0.47 standard deviation (SD) and for artifacts overall was 4.4 ± 0.5 SD. Mild to moderate respiratory motion artifacts were seen in three patients (3 of 20, 15%) on T1-weighted post-contrast images with a mean IQ score of 4.8 ± 0.52 (Fig. 3). Mild motion artifacts were observed in four patients (5 of 20, 25%) on DWI with a mean IQ score of 4.75 ± 0.44 . The mean examination time was 27.4 ± 6.5 min for chest, abdomen and pelvis and 21.0 ± 6.9 min for abdomen and pelvis. The mean score of patient satisfaction regarding exam duration was 6.45 ± 2.19 (median, 6) and did not correlate with scan duration.

Conclusion

MR scanning with the automated Whole-Body Dot Engine results in good to excellent image quality within a reasonable total examination time with only small patient-dependent variations. An almost 'single-button protocol' for standardized fast, reproducible, and automated workflow of chest, abdomen, and pelvis could open up new possibilities in the diagnostic process. However, further comparison studies with traditional manual scan modes need to be performed to support our preliminary experience.

Contact

Cäcilia Reiner, M.D.

Institute of Diagnostic and
Interventional Radiology
University Hospital Zurich

Raemistrasse 100
8091 Zurich, Switzerland
caecilia.reiner@usz.ch



References

- Andreisek G. Point-of-Care MR Imaging and how we can learn from other imaging modalities. Thoughts on a potential new strategy. *MAGNETOM Flash* (63) 3/2015:4-7. siemens-healthineers.us/vida-flash
- Stemmer A, Kiefer B. Combination of integrated slice-specific dynamic shimming and pixel-wise unwarping of residual EPI distortions. *Proc Intl Soc Mag Reson Med*. 2015;23:3729.

Try them on your system

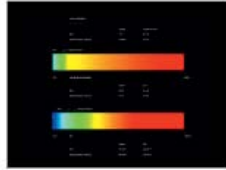
Trial licenses for many of the applications featured in this issue of MAGNETOM Flash are available free of charge for a period of 90 days.



Tim Planning Suite

Allows planning of several stations at once, e.g. on composed localizer images. >

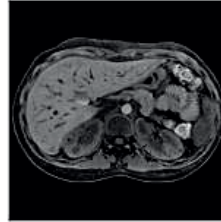
Tim Planning Suite



LiverLab

Evaluating the iron and fat content of the liver is an important step in monitoring early stages of liver diseases. >

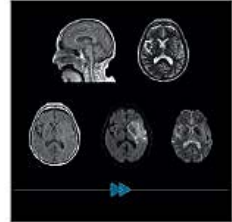
LiverLab



FREEZEit

Embrace motion in liver imaging. >

FREEZEit



GOBrain

Push-button brain exam in 5 minutes.* >

CAIPIRINHA



Brain Dot Engine

The Brain Dot Engine increases productivity and standardization with guided and automated workflows. >

Brain Dot Engine



Abdomen Dot Engine

The Abdomen Dot Engine is customized for dynamic liver examinations and consistent contrast timing. >

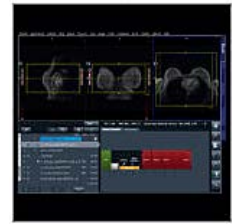
Abdomen Dot Engine



Spine Dot Engine

The Spine Dot Engine optimizes cervical, thoracic, and lumbar spine imaging for a wide range of patients and conditions. >

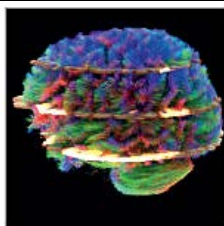
Spine Dot Engine



Breast Dot Engine

The Breast Dot Engine supports consistent frequency selection for fat, water, saline or silicone. >

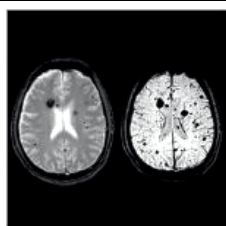
Breast Dot Engine



Simultaneous Multi-Slice

Accelerate advanced neuro applications for clinical routine. >

Simultaneous Multi-Slice



SWI

SWI is a new type of contrast technique in MRI that detects blood and iron deposits better than conventional methods. >

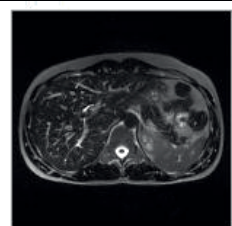
SWI



Advanced WARP

Advanced WARP corrects in- and through-plane distortions for more accurate diagnosis of tissue surrounding orthopedic implants. >

Advanced WARP



SPACE

SPACE enables the acquisition of high resolution 3D datasets. >

SPACE

For further details, product overviews, image galleries, step-by-step videos and general requirements visit us at:

[siemens-healthineers.us/mri-options-overview](https://www.siemens-healthineers.us/mri-options-overview)

Compressed Sensing: a Paradigm Shift in MRI

Christoph Forman¹; Jens Wetzl²; Dominik Nickel¹; Robert Grimm¹; Carmel Hayes¹; Michaela Schmidt¹

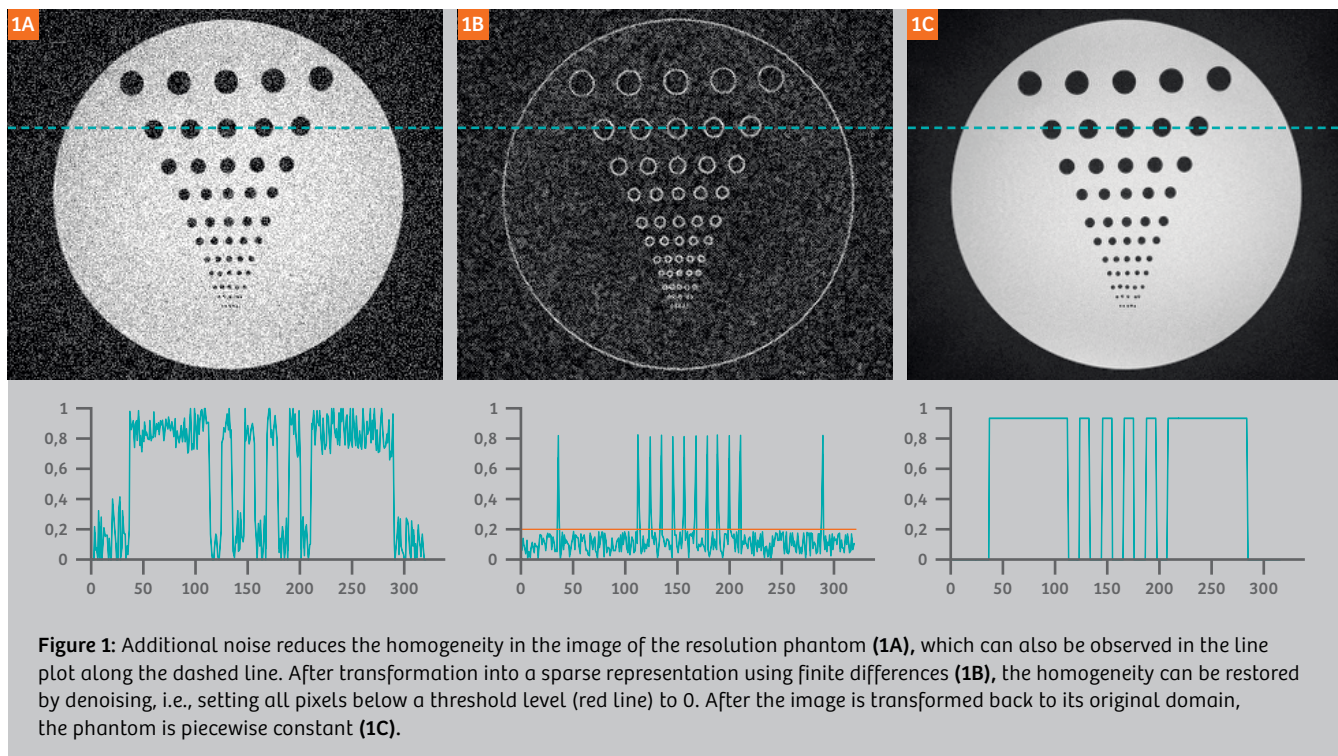
¹Siemens Healthineers, Magnetic Resonance, Erlangen, Germany

²Pattern Recognition Lab, Friedrich-Alexander-University Erlangen-Nuremberg, Erlangen, Germany

Introduction

Reducing the complexity and length of examinations has been a major direction of research in magnetic resonance imaging (MRI) in recent years. With the introduction of the Dot engines, the complexity of MR examinations could be reduced through automatization and guidance, providing standardized and time-efficient workflows. Considerable effort has also been spent on developing methods to speed up data acquisition without degrading image quality. Accelerated imaging is a key factor to enable the visualization of rapid physiological or contrast changes in dynamic imaging. Moreover, short scans reduce the risk of artifacts due to any kind of motion during the scan.

A significant speed-up of data acquisition allows both respiratory and cardiac motion to be frozen while maintaining an adequate temporal and spatial resolution. This in turn results in a high-quality and robust examination even for uncooperative patients, since data acquisition may be performed in free breathing. Furthermore, reduced scan time and a decreased number of breath-holds improve patient comfort. Last but not least, accelerated imaging means shorter examinations that can be invested in additional scans, higher resolution, or to improve the overall patient throughput. In this context, parallel imaging and compressed sensing techniques have been proposed to significantly speed up the acquisition time while maintaining diagnostic image quality.



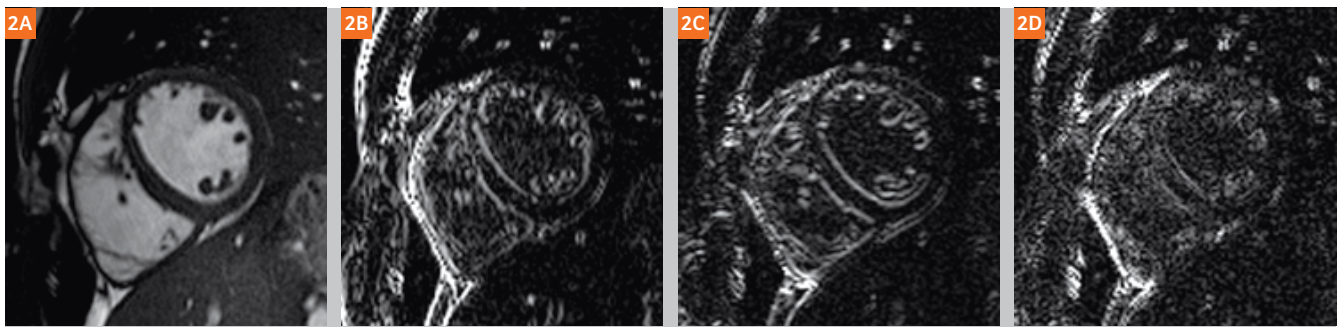


Figure 2: The short-axis view of the heart (2A) is transformed by the wavelet transform to achieve a sparse representation. In addition to the low-resolution representation of the original image, the wavelet transform results in three edge images (2B–2D): While (2B) and (2C) contain the edges in horizontal and vertical direction, respectively, Figure 2D shows the diagonal edge components of the image. In the wavelet domain, the content of the image is sufficiently described by only few coefficients, i.e. the bright pixels.

Parallel imaging

Parallel imaging [1, 2] is well established in current clinical practice to speed up data acquisition in a large number of applications. With this technique, scan acceleration is usually achieved by uniformly sub-sampling k -space, for example, by skipping every other line. The resulting aliasing can be unfolded by incorporating the spatial encoding capabilities of multi-coil receiver arrays. However, the scan time reduction is often restricted to moderate acceleration factors between 2 and 4. This limitation is due to the restricted encoding capabilities in terms of number and position of the receiver coils. Additionally, acquiring less data also leads to a reduced signal-to-noise ratio (SNR).

Compressed sensing

In recent years, compressed sensing has gained large scientific attention. Originally, it was proposed as a general concept to accurately reconstruct a signal from a small number of random measurements [3, 4]. A few years later, compressed sensing was introduced to MRI [5] and successfully combined with parallel imaging [6, 7]. Exploiting the compressibility of medical images, this method promises to markedly exceed the acceleration rates that are feasible with parallel imaging. Although compressed sensing has denoising properties, it also has to deal with SNR loss from scan acceleration. Hence, possible acceleration factors scale with the native SNR of the scan. Up to now, the potential of compressed sensing has been shown in a large number of applications from 2D to 5D imaging [8–16].

The successful utilization of compressed sensing is a team play of data acquisition and image reconstruction. In the paper introducing compressed sensing to MRI, three criteria were identified as being essential to ensure successful image recovery from sub-sampled data [5]:

- First, the object that is acquired should have a *sparse representation* after conversion with a mathematical transformation.

- Second, k -space should be sub-sampled such that the aliasing results in *incoherent*, i.e. noise-like, artifacts in the image.
- Finally, image reconstruction requires a *nonlinear, iterative optimization* that simultaneously enforces a sparse representation of the resulting image. Thereby, it removes the noise-like artifacts, while it preserves its consistency to the acquired data.

These three essential requirements are discussed in detail below.

Transform sparsity

An image is considered as sparse when its informational content is represented by only a few pixels, while the contribution of the remaining majority of pixels is close to zero. In medical imaging, an angiogram provides a good example for such a sparse representation. However, in MRI, not all images are inherently sparse. But these images can also have a sparse representation utilizing a sparsifying transform. This transform provides an invertible mapping from an image to a sparse representation. Finite differences, i.e. images that contain only edge information, provide a simple technique to achieve a sparse representation, if the image is piecewise constant as shown in Figure 1. Discrete cosine transform and discrete wavelet transform are frequently used in the context of image compression, for example, in JPEG image compression. Utilizing such methods, images may be transformed into a sparse representation (see Fig. 2). In this domain, the content of the image is sufficiently described by only few coefficients, i.e. the bright pixels. The percentage of these pixels relative to the total number of pixels defines the sparsity of the image. For image compression, pixels in this sparse representation that are below a certain threshold can be set to zero, which facilitates a compression of the signal. Once the compressed signal is converted back to its initial domain, the visual difference between the resulting image and its original version is negligible. In particular, the discrete wavelet transform has been shown to be a suitable

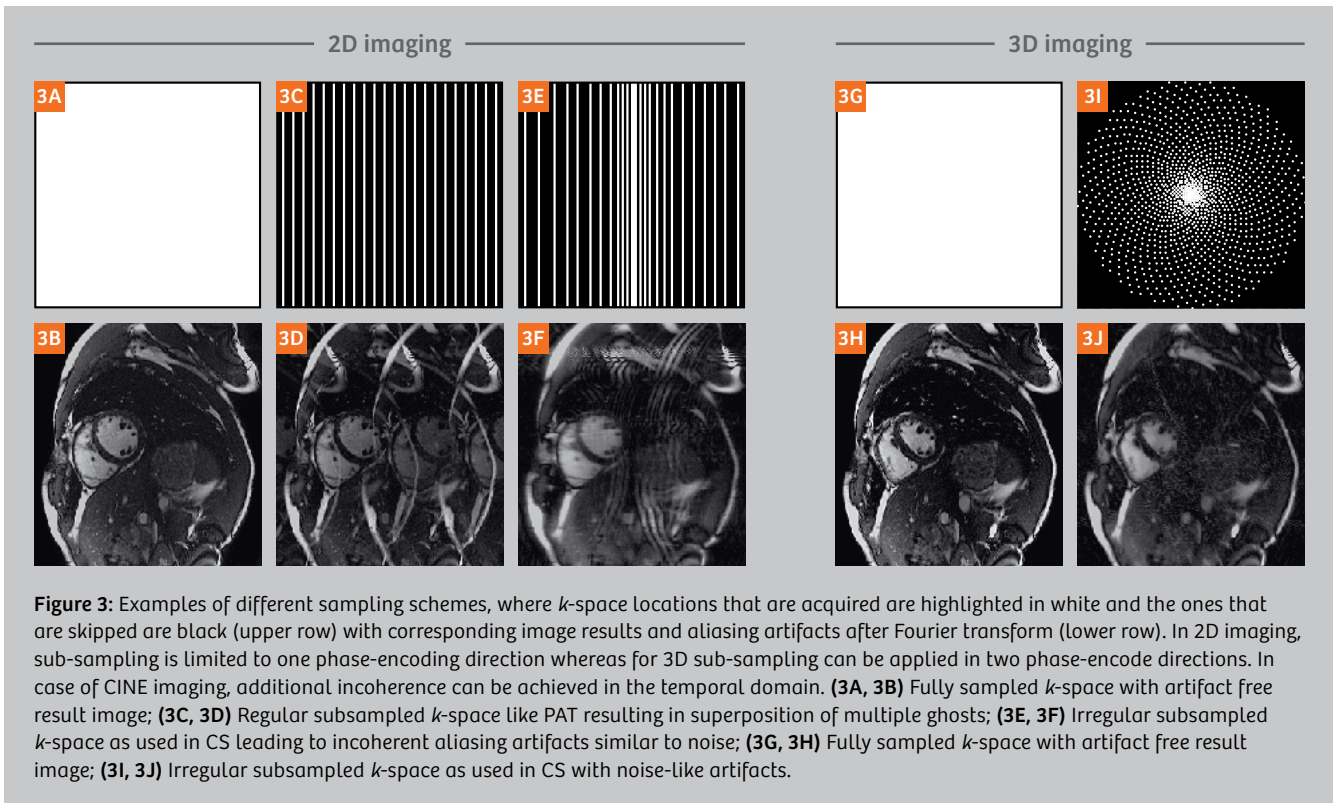


Figure 3: Examples of different sampling schemes, where k -space locations that are acquired are highlighted in white and the ones that are skipped are black (upper row) with corresponding image results and aliasing artifacts after Fourier transform (lower row). In 2D imaging, sub-sampling is limited to one phase-encoding direction whereas for 3D sub-sampling can be applied in two phase-encode directions. In case of CINE imaging, additional incoherence can be achieved in the temporal domain. **(3A, 3B)** Fully sampled k -space with artifact free result image; **(3C, 3D)** Regular subsampled k -space like PAT resulting in superposition of multiple ghosts; **(3E, 3F)** Irregular subsampled k -space as used in CS leading to incoherent aliasing artifacts similar to noise; **(3G, 3H)** Fully sampled k -space with artifact free result image; **(3I, 3J)** Irregular subsampled k -space as used in CS with noise-like artifacts.

sparsifying transform for many natural images, including MRI images, and is commonly used in compressed sensing applications. In the case of dynamic imaging, including CINE imaging, this transform can also be applied in the temporal dimension. The redundancy of information along this temporal dimension can be exploited, and often the sparsity is even higher compared to the spatial dimensions.

Incoherent sampling

Unlike the regular sub-sampling patterns used for parallel imaging, the data acquisition process for compressed sensing requires that k -space sub-sampling is irregular (see Fig. 3C for regular and 3E, 3I for irregular sampling). In conventional Cartesian parallel imaging, regular sub-sampling of k -space is advantageous in that the phase-encoding gradient is increasing linearly during the measurement, which is beneficial for physical and MRI hardware limitation reasons. However, violating the Nyquist sampling theorem in this manner results in a superposition of shifted replicas of the original signal as illustrated in Figure 3D. The number of replicas equals the chosen sub-sampling rate. This aliasing can then be unfolded utilizing the spatial encoding capabilities of the multi-coil receiver array and parallel imaging. In contrast, irregular, incoherent sub-sampling of k -space, as required for compressed sensing, would result in a noise-like appearance of sub-sampling artifacts (see Figs. 3F, 3J). Theoretically, completely random sub-sampling is optimal to ensure this noise-like behavior. However, purely random sampling

is impractical in the case of MRI. On the one hand, large and random steps in k -space may require large-amplitude gradient steps and should be avoided due to hardware limitations and physical reasons. On the other hand, the sampling trajectory must be repeatable to allow the same acquisition to be reproduced with consistent image quality. Therefore, sub-sampling patterns featuring deterministic properties that mimic random sampling within the given constraints are frequently used for compressed sensing data acquisition. In 2D Cartesian imaging with pure spatial coverage, the sub-sampling is limited to one dimension, as only the phase-encoding direction is sub-sampled in MRI. But in case of 2D dynamic imaging, the sampling pattern can be varied from one time frame to the next in order to maintain sufficient incoherence for compressed sensing. In 3D Cartesian imaging, sub-sampling can be applied in two phase-encoding directions. Alternatively, non-Cartesian sampling trajectories can be used, e.g., radial or spiral imaging, that already facilitate an incoherent sampling of k -space for 2D imaging.

Nonlinear image reconstruction

If the two above-mentioned requirements are sufficiently met, the image can be recovered from the sub-sampled data by nonlinear, iterative reconstruction. In this reconstruction, a data fidelity term ensures consistency of the estimated image to the acquired data and a transform sparsity term enforces a sparse representation of the image in the transform domain by solving the following equation:

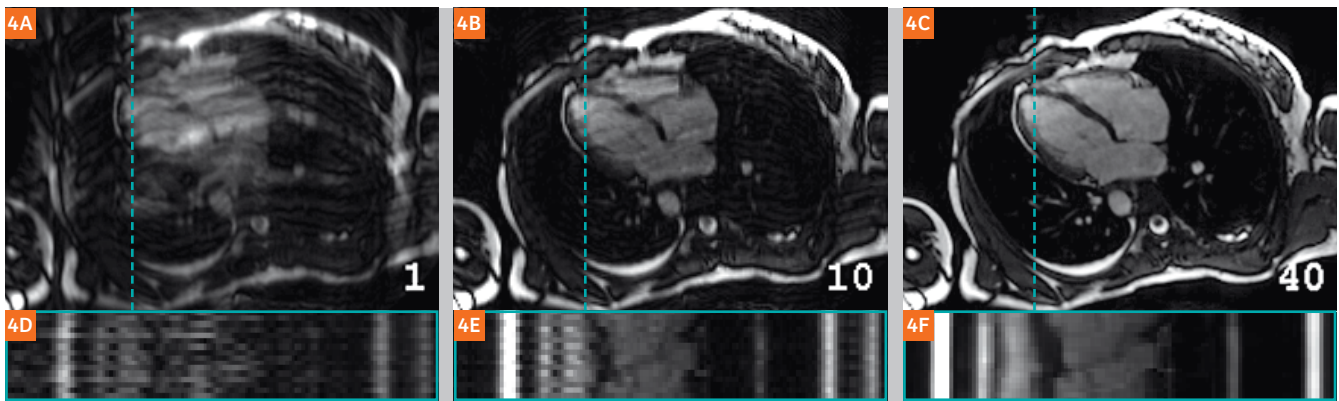


Figure 4: This Figure shows the progress of the optimization procedure to preserve data fidelity and reduce noise-like artifacts exemplarily in a Cardiac 2D CINE dataset (4A–4C). While the top image shows one image of the time series, a temporal profile along the dashed line is plotted below. The incoherent sub-sampling in the spatio-temporal domain results in incoherent artifacts that dominate the image after the first iteration (4A). Enforcing a sparse representation of the image and exploiting temporal redundancy, these artifacts are reduced with an increasing number of iterations (4B). The compressed sensing reconstruction is terminated after 40 iterations and results in an aliasing-free image (4C).

$$\min_x \underbrace{\|Ax - y\|_2^2}_{\text{data fidelity}} + \lambda \underbrace{\|\Phi(x)\|_1}_{\text{transform sparsity}}$$

The data fidelity term minimizes the least-squares difference ($\| \cdot \|_2^2$) between the estimated image, x , and the acquired k -space data, y . The system matrix, A , describes the data acquisition process, i.e., the transform from spatio-temporal to frequency domain, which is required for the comparison of the image and acquired data. Incorporating parallel imaging, it consists of the coil sensitivity maps of the individual receiver coil elements, the Fourier transform, and the applied sub-sampling pattern during data acquisition. In the transform sparsity term, the image is transformed into a sparse representation by (\cdot) , for example, using the discrete wavelet transform. In this term, the sum of the absolute values of the pixels in the transform domain, denoted by the ℓ_1 norm ($\| \cdot \|_1$), is minimized. Hence, the optimization procedure minimizing this equation seeks to find a solution that fulfills both criteria, data consistency and transform sparsity. This optimization procedure is more computationally intensive than conventional reconstruction, e.g., parallel imaging. The balance between data fidelity and sparsity is adjusted with the regularization parameter, which is usually found empirically. While small values of λ lead to an image that is closer to the acquired data, increasing this value tends to produce an image that is in favor of the sparse solution. When λ is too low, the image will be noisy, and when λ is too high a strongly filtered image appearance may be the consequence. The equation described above is iteratively minimized until a convergence criterion is met or a fixed number of iterations is reached. Figure 4 illustrates this optimization in the example of real-time CINE imaging of the heart.

Transition into clinical routine

Compressed sensing acquisition and reconstruction have been completely integrated into our clinical MRI scanners. The additional parameters needed to compose the compressed sensing protocols, for both acquisition and reconstruction, have been seamlessly integrated into our user interface (UI). A selection of possible continuous acceleration factors takes the place of discrete numbers that were familiar from parallel imaging. This facilitates a UI experience with a low level of complexity. The award-winning algorithm for compressed sensing reconstruction [9], ranking first at the ISMRM 2014 “sub-Nyquist” reconstruction challenge, has been fully integrated into the Siemens image reconstruction environment. Without the need for additional hardware, the images are directly calculated inline utilizing the full computational power of the reconstruction computer. Compressed sensing reconstruction is performed on a graphics processing unit, which provides a significant speed-up in processing time. For example, the image series of one cardiac real-time CINE slice is processed in 10 to 15 seconds.

Thanks to its high acceleration rate due to compressed sensing, real-time sequences allow for a temporal and spatial resolution comparable to that of conventional segmented acquisitions. For example, compressed sensing in cardiac imaging permits fast quantification of left-ventricular (LV) function in a single breath-hold [26]. As demonstrated in Figure 5, this sequence still provides diagnostic images for LV function quantification even in challenging scenarios, such as in the presence of arrhythmia, where conventional sequences usually fail. This sequence may also be applied in free breathing, which is beneficial for patients who are not able to hold their breath sufficiently and, in general, allows for a simplified and more patient-friendly examination workflow.

A new experience of time-resolved 3D dynamic imaging is planned, Golden-angle Radial Sparse Parallel (GRASP) MRI, which extends and exploits a time-resolved compressed sensing reconstruction. As a consequence the advantages of two worlds are obtained: The motion robustness of the StarVIBE and the high temporal resolution of a time-resolved compressed sensing reconstruction TWIST-VIBE [28]. GRASP-VIBE even allows reconstructions with varying temporal resolution over the course of an acquisition, and support of auto-bolus detection. These features can be used, e.g. in liver imaging to set the desired temporal resolution for the pre-contrast, arterial, portal-venous and delayed phase individually. An example is shown in Figure 6.

Conclusion

Compressed sensing facilitates rapid MR imaging by exploiting the fact that medical images have a sparse representation in a certain transfer domain. Representing a team play of data acquisition and image reconstruction, this allows for the reconstruction of artifact-free images following incoherent data acquisition. The acceleration enables a reduction in the acquisition time or an improvement in the spatial and/or temporal resolution. Real-time imaging featuring compressed sensing helps to reduce the need for breath-holding or ECG triggering. The integration of protocols based on compressed sensing in clinical workflows allows a significant reduction in the examination time for each patient. Our generalized integration of compressed sensing in the scanner environment will allow for the straightforward introduction of further applications that are likely to come in the near future.

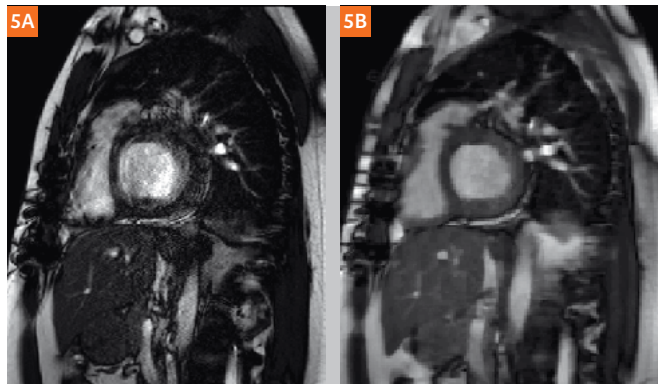


Figure 5: In cardiac imaging, the high acceleration rate due to compressed sensing enables real-time CINE imaging with a temporal and spatial resolution in a comparable range as conventional segmented acquisitions. While conventional imaging might fail in challenging scenarios, like in case of arrhythmia (**5A**), the compressed sensing real-time sequence preserves a diagnostic image quality that still enables the quantification of LV function (**5B**). Images courtesy of Dr. François Pontana, Lille University Hospital, Lille, France.

References

- ¹M. A. Griswold, P. M. Jakob, R. M. Heidemann, M. Nittka, V. Jellus, J. Wang, B. Kiefer, and A. Haase. "Generalized Autocalibrating Partially Parallel Acquisitions (GRAPPA)". *Magnetic Resonance in Medicine*, Vol. 47, No. 6, pp. 1202–1210, June 2002.
- ²K. Pruessmann, M. Weiger, M. B. Scheidegger, and P. Boesiger. "SENSE: Sensitivity Encoding for Fast MRI". *Magnetic Resonance in Medicine*, Vol. 42, No. 5, pp. 952–962, Nov. 1999.
- ³D. Donoho. "Compressed Sensing". *IEEE Transactions on Information Theory*, Vol. 52, No. 4, pp. 1289–1306, Apr. 2006.

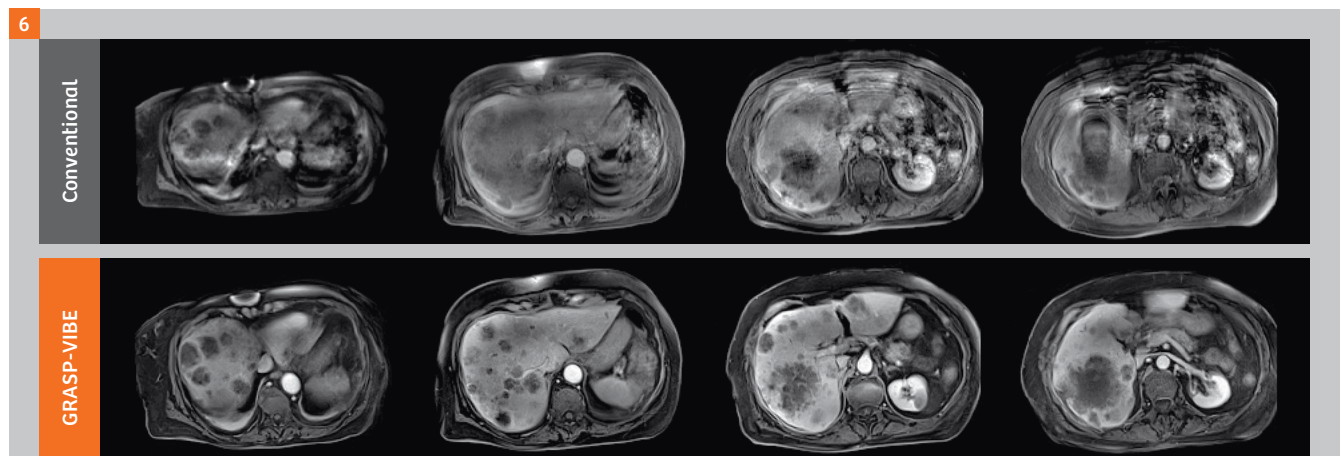


Figure 6: Conventional VIBE and GRASP-VIBE of a 82-year-old female patient with dementia, unable to hold her breath. Images courtesy of Universitätsspital Basel, Switzerland.

- ⁴E. Candes and J. Romberg. "Sparsity and incoherence in compressive sampling". *Inverse problems*, Vol. 23, No. 3, pp. 969–985, Apr. 2007.
- ⁵M. Lustig, D. Donoho, and J. M. Pauly. "Sparse MRI: The Application of Compressed Sensing for Rapid MR Imaging". *Magnetic Resonance in Medicine*, Vol. 58, No. 6, pp. 1182–1195, Dec. 2007.
- ⁶D. Liang, B. Liu, J. Wang, and L. Ying. "Accelerating SENSE Using Compressed Sensing". *Magnetic Resonance in Medicine*, Vol. 62, No. 6, pp. 1574–1584, Dec. 2009.
- ⁷Block, K. T., Uecker, M. and Frahm, J., "Undersampled radial MRI with multiple coils. Iterative image reconstruction using a total variation constraint", *Magnetic Resonance in Medicine*, Vol. 57, No. 6, pp. 1086–1098, May 2007.
- ⁸G. Adluru, L. Chen, S. Kim, N. Burgon, E. G. Kholmovski, N. F. Marrouche, and E. V. R. DiBella. "Three-dimensional late gadolinium enhancement imaging of the left atrium with a hybrid radial acquisition and compressed sensing". *Journal of Magnetic Resonance Imaging*, Vol. 34, No. 6, pp. 1465–1471, Dec. 2011.
- ⁹J. Liu, J. Rapin, T.-C. Chang, A. Lefebvre, M. O. Zenge, E. Mueller, and M. S. Nadar. "Dynamic cardiac MRI reconstruction with weighted redundant Haar wavelets". In: *Proceedings of the 20th Annual Meeting of ISMRM*, p. 4249, Melbourne, Australia, May 2012.
- ¹⁰F. Han, S. Rapacchi, S. Kahn, I. Ayad, I. Salusky, S. Gabriel, A. Plotnik, J. P. Finn, and P. Hu, "Four-dimensional, multiphase, steady-state imaging with contrast enhancement (MUSIC) in the heart: A feasibility study in children". *Magnetic Resonance in Medicine*, Vol. 74, No. 4, pp. 1042–1049, Oct. 2015.
- ¹¹S. T. Ting, R. Ahmad, N. Jin, J. Craft, J. Serafim da Silveira, H. Xue, and O. P. Simonetti. "Fast Implementation for Compressive Recovery of Highly Accelerated Cardiac Cine MRI Using the Balanced Sparse Model". *Magnetic Resonance in Medicine*, doi: 10.1002/mrm.26224.
- ¹²D. Stäb, T. Wech, F. A. Breuer, A. M. Weng, C. O. Ritter, D. Hahn, and H. Köstler, "High resolution myocardial first-pass perfusion imaging with extended anatomic coverage". *Journal of Magnetic Resonance Imaging*, Vol. 39, No. 6, pp. 1575–1587, Jun. 2014.
- ¹³X. Chen, M. Salerno, Y. Yang, and F. H. Epstein, "Motion-compensated compressed sensing for dynamic contrast-enhanced MRI using regional spatiotemporal sparsity and region tracking: Block low-rank sparsity with motion-guidance (BLOSM)", *Magnetic Resonance in Medicine*, Vol. 72, No. 4, pp. 1028–1038, Oct 2014.
- ¹⁴H. Xue, S. Inati, S. Sørensen, P. Kellman, and M. S. Hansen, "Distributed MRI Reconstruction Using Gadgetron-Based Cloud Computing", *Magnetic Resonance in Medicine*, Vol. 73, No. 3, pp. 1015–1025, March 2015.
- ¹⁵J. Wetzl, F. Lugauer, M. Schmidt, A. Maier, J. Hornegger, and C. Forman. "Free-Breathing, Self-Navigated Isotropic 3-D CINE Imaging of the Whole Heart Using Cartesian Sampling", In: *Proceedings of the 24th Annual Meeting of ISMRM*, p. 411, Singapore, May 2016.
- ¹⁶L. Feng, L. Axel, H. Chandarana, K. T. Block, D. K. Sodickson, and R. Otazo. "XD-GRASP: Golden-angle radial MRI with reconstruction of extra motion-state dimensions using compressed sensing". *Magnetic Resonance in Medicine*, Vol. 75, No. 2, pp. 775–788, Feb. 2016.
- ¹⁷C. Forman, D. Piccini, R. Grimm, J. Hutter, J. Hornegger, and M.O. Zenge. "Reduction of respiratory motion artifacts for free-breathing whole-heart coronary MRA by weighted iterative reconstruction", *Magnetic Resonance in Medicine*, Vol. 73, No. 5, pp. 1885–1895, May 2015.
- ¹⁸A. F. Stalder, M. Schmidt, H. H. Quick, M. Schlamann, S. Maderwald, P. Schmitt, Q. Wang, M. S. Nadar, and M. O. Zenge. "Highly under-sampled contrast-enhanced MRA with iterative reconstruction: Integration in a clinical setting", *Magnetic Resonance in Medicine*, Vol. 74, No. 6, pp. 1652–1660, Dec. 2015.
- ¹⁹T. Yamamoto, K. Fujimoto, T. Okada, Y. Fushimi, A. Stalder, Y. Natsuaki, M. Schmidt, and K Togashi, "Time-of-Flight Magnetic Resonance Angiography With Sparse Undersampling and Iterative Reconstruction: Comparison With Conventional Parallel Imaging for Accelerated Imaging", *Investigative Radiology*, Vol. 51, No. 6, pp. 372–378, Jun 2016.
- ²⁰J. Wetzl, C. Forman, B. J. Wintersperger, L. D'Errico, M. Schmidt, B. Mailhe, A. Maier, and A. F. Stalder. "High-resolution dynamic CE-MRA of the thorax enabled by iterative TWIST reconstruction", *Magnetic Resonance in Medicine*, doi: 10.1002/mrm.26146.
- ²¹E. Mussard, T. Hilbert, R. Meuli, J.-P. Thiran, and T. Kober. "Accelerated MP2RAGE Imaging Using Sparse Iterative Reconstruction", In: *Proceedings of the 24th Annual Meeting of ISMRM*, p. 4216, Singapore, May 2016.
- ²²R. Otazo, M. Nittka, M. Bruno, E. Raithel, C. Geppert, S. Gyftopoulos, M. Recht, and L. Rybak. "Sparse-SEMAC: Rapid and Improved SEMAC Metal Implant Imaging Using SPARSE-SENSE Acceleration", *Magnetic Resonance Imaging*, July 2016, Early View, DOI: 10.1002/mrm.26342.
- ²³J. Fritz, S. Ahlawat, S. Demehri, G.K. Thawait, E. Raithel, W.D. Gilson, M. Nittka. "Compressed Sensing SEMAC: 8-fold Accelerated High Resolution Metal Artifact Reduction MRI of Cobalt-Chromium Knee Arthroplasty Implants", *Investigative Radiology*, October 2016, Vol. 51, Issue 10, pp 666–676.
- ²⁴J. Fritz, E. Raithel, G. K. Thawait, W. Gilson, and D. F. Papp. "Six-Fold Acceleration of High-Spatial Resolution 3D SPACE MRI of the Knee Through Incoherent k-Space Under-sampling and Iterative Reconstruction – First Experience". *Investigative Radiology*, Vol. 51, No. 6, pp. 400–409, Jun 2016.
- ²⁵D. Nickel, X. Chen, B. Mailhe, Q. Wang, Y. Son, J. M. Lee, and B. Kiefer. "Motion-resolved 3D dynamic contrast enhanced liver MRI", In: *Proceedings of the 24th Annual Meeting of ISMRM*, p. 4253, Singapore, May 2016.
- ²⁶G. Vincenti, P. Monney, J. Chaptinel, T. Rutz, S. Coppo, M.O. Zenge, M. Schmidt, M.S. Nadar, D. Piccini, P. Chèvre, M. Stuber, and J. Schwitler, "Compressed Sensing Single-Breath-Hold CMR for Fast Quantification of LV Function, Volumes, and Mass" *JACC: Cardiovascular Imaging*, Vol. 7, No. 9, pp. 882–892, Sep. 2014.
- ²⁷L. Feng, R. Grimm, T.K. Block, H. Chandarana, S. Kim, J. Xu, L. Axel, D.K. Sodickson, and R. Otazo, "Golden-angle radial sparse parallel MRI: combination of compressed sensing, parallel imaging, and golden-angle radial sampling for fast and flexible dynamic volumetric MRI", *Magnetic Resonance in Medicine*, Vol. 72, No. 3, pp. 707–17, September 2014.
- ²⁸H. Chandarana, L. Feng, T.K. Block, A.B. Rosenkrantz, R.P. Lim, J.S. Babb, D.K. Sodickson, and R. Otazo, "Free-Breathing Contrast-Enhanced Multiphase MRI of the Liver Using a Combination of Compressed Sensing, Parallel Imaging, and Golden-Angle Radial Sampling", *Investigative Radiology*, Vol. 48, No. 1, pp. 10–16, January 2013.

Contact



Christoph Forman
Siemens Healthcare GmbH
HC DI MR PI TIO CARD
Postbox 32 60
91050 Erlangen
Germany
christoph.forman@siemens-healthineers.com

syngo MR XA10—Your New Work Environment for More Comfortable Scanning and Intuitive Image Processing

Alexander Aulesjord; Gregor Thörmer, Ph.D.

Siemens Healthineers, Erlangen, Germany

To counter falling reimbursement and increasing cost pressure many imaging facilities seek ways to both increase productivity and patient throughput. One example of these efforts can be seen directly in the continuously increasing number of patients scheduled for MRI per hour over the course of the last years.

Higher patient throughput not only increases the technologists' workload but also their expectations towards the tools available to them. The user interface (UI) to the MR scanner is arguably the most important tool that technologists have at their disposal. Most interactions with the MR scanner over the course of the examination will happen via the UI. As such, the UI can have substantial influence over how productive an MR scanner is operated. Great care should be taken such that when designing a new UI, it will be easy to navigate, task cards for scanning and processing should not overlap, and the workflow should follow the natural course of the MR examination.

It is also crucial to carefully preserve the overall functionality and the known appearance of any new software, be it in MR technology or consumer electronics, in order to make the transition to a new UI for experienced users easy.

Our new 3T MRI system, MAGNETOM Vida, introduces a completely redesigned MR UI running on a new hardware platform. Evolving from the successful *syngo*® MR E11 platform, the new *syngo* MR XA10 software¹ is a user-centric control center for patient registration, scanning, post-processing, and result distribution.

Dual monitor setup

Studies have shown that even standard office applications substantially benefit from a dual monitor setup, resulting in 45% easier task tracking, 32% higher performance, and 24% more comfortable use than single monitor setups [1].

To ease the work of the MR technologist in a similar manner, *syngo* MR XA10 software operates on a dual monitor scanning workplace with two large 24-inch monitors with a reorganized user interface.

For a more natural scanning and viewing process, different tasks have been clearly separated: The left screen is reserved for patient registration, scanning, and protocol management, while the right screen, especially with the new MR View&GO application which encompasses reconstructions, post-processing, image quality check, and distribution of results to the PACS and other DICOM nodes (Fig. 1). This dual monitor setup, with separated scan and viewing monitors, makes for a more natural working environment in which the technologist has a complete overview of the examination and results. Constant context switches and distractions are reduced, enabling stronger focus on the patient and true multitasking for increased quality and productivity.

syngo MR XA10 builds on the established *syngo* MR E11 platform, inheriting many known features and UI elements, which makes orientation for users of the existing platform easy. As shown in Figure 2, central UI elements and features on the left screen have been preserved but newly arranged on the larger monitor. Furthermore, the new layout now provides fixed positions for UI elements like the physio display and the inline display. Other useful components like the Dot Cockpit for protocol management have not been changed in their appearance. They do, however, offer the ability to be opened on the right monitor while scanning, therefore not interfering with other processes.



Figure 1: Dual monitor setup with two 24-inch screens. Clear task separation with image acquisition on the left-hand side and processing with MR View&GO on the right-hand side.



Figure 2: The new workplace with syngo MR XA10 (2B) evolves from syngo MR E11. Planning segments (orange), queue (yellow), scan parameters (purple) have kept their appearance but were newly arranged. The new layout provides fixed positions for hovering UI elements such as the physio display and the inline display (blue).

“The new interface is clearly structured. It is easy to get used to it.”

Andreas Lingg, MTRA
Tübingen University Hospital, Tübingen, Germany

“The statements by the Siemens Healthineers customer presented herein are based on results that were achieved in the customer’s unique setting. Since there is no “typical” hospital and many variables exist (e.g., hospital size, case mix, level of IT adoption), there can be no guarantee that other customers will achieve the same results.”

Right-hand side with MR View&GO

MR View&GO is a dedicated MR viewer that allows viewing, routine post-processing, filming and result distribution in one comprehensive workflow with consecutive steps (Fig. 3A). As soon as a patient has been registered on the left-hand side, a corresponding MR View&GO automatically opens for the respective patient on the right-hand side. Every scan that has been acquired and reconstructed automatically appears on the right screen.

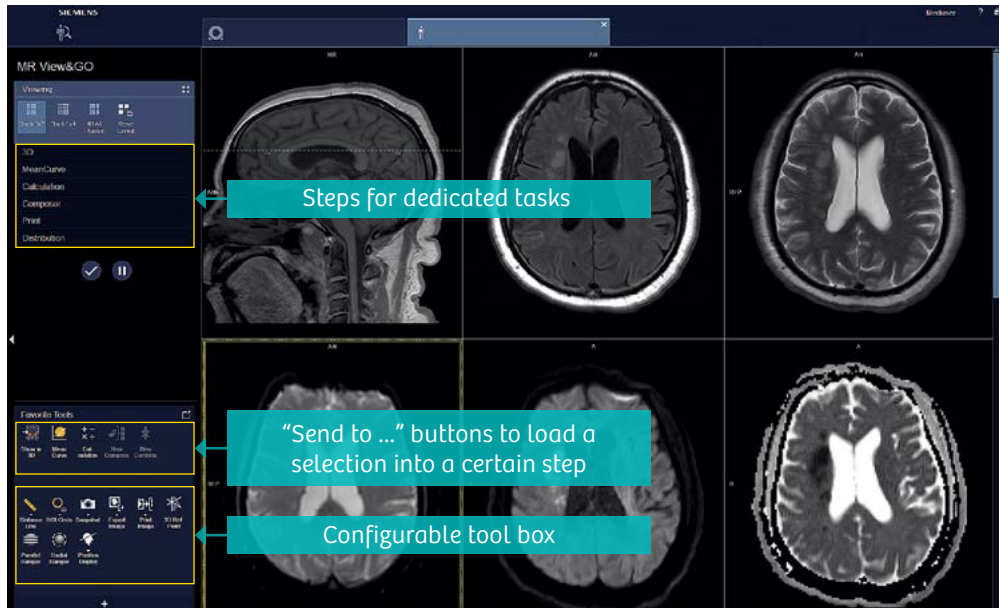


Figure 3A: MR View&GO is a dedicated viewer for MR studies, offering consecutive steps for image viewing, processing and distribution. The user can configure an individual tool box of frequently used features such as image markers, distance measurements or ROI analysis in the lower left corner. Further analysis tools can be found in so-called “corner menus” in the edges of individual image segments.

Pre-processing with Recon&GO

Powerful image pre-processing capabilities, e.g. automatic InlineSubtraction of dynamic series, InlineMPR calculation of 3D datasets or InlineComposing of multi-station exams, which are all standard, run automatically in the background. This helps to reduce the workload for the MR technologist.

Step-by-step from quality control to distribution

Following the natural workflow, MR View&GO guides you from basic viewing and quality control towards result distribution to the PACS and other DICOM nodes (Fig. 3B). Intermediate post-processing steps which might be indicated depending on the case can be easily launched by selecting an image series and transferring it to the respective step with one mouse click.

This, for example, enables the reformatting of images in 3D as Multiplanar Reconstructions (MPR), Maximum Intensity Projection (MIP), or with a Volume Rendering Technique (VRT). Furthermore, arithmetic image analysis or the interactive extrapolation of very high b-values (up to 5000 s/mm²) can be easily performed while the scan is running. The resulting images, for example multiplanar reconstructions of a 3D dataset, can be easily dragged-and-dropped back to the planning segments on the left monitor to precisely plan subsequent scans.

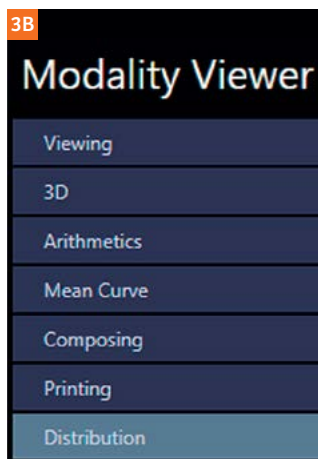


Figure 3B: MR View&GO offers consecutive steps to guide you from basic quality control through potential further processing steps towards result distribution. To launch a specific step, e.g. the 3D card, you only have to select a series of images and press the “Show in 3D” button on the left-hand side (see Figure 3A).

To evaluate dynamically acquired contrast-enhanced image series, MR View&GO also offers a dedicated MeanCurve analysis step as a standard feature. This, for example, helps in the evaluation of a test-bolus scan, prostate DCE series (Fig. 4) or contrast-enhanced breast MRI.

In addition to InlineComposing, MR View&GO provides manual composing for complex cases to support, e.g., whole-spine, whole-body, or angiography exams.

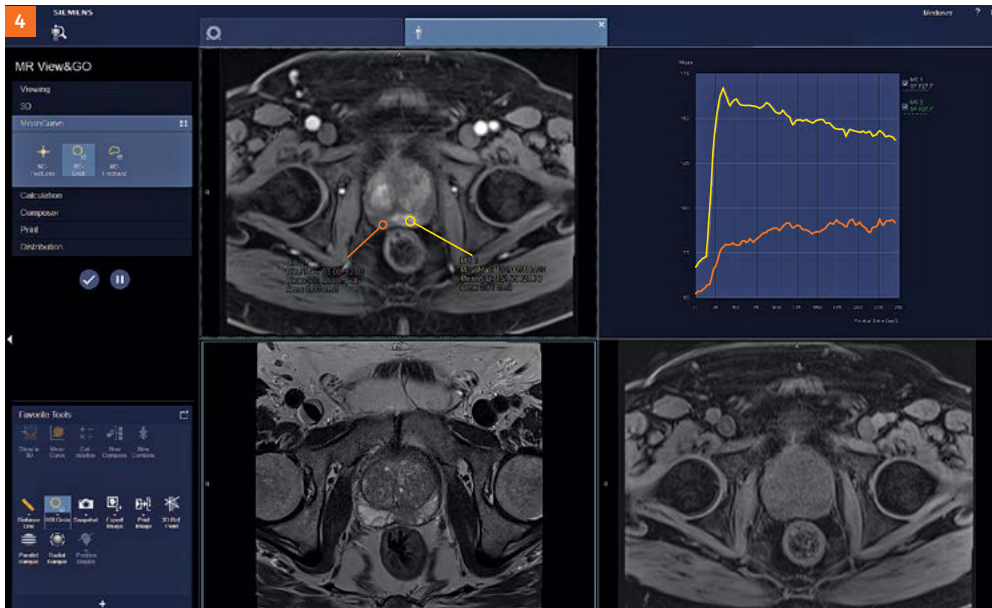


Figure 4: The standard MeanCurve analysis step for evaluation of the dynamic behavior of contrast enhancement in tissues. As shown in this example of a patient with prostate cancer, ROIs have been placed in the peripheral zone, illustrating fast wash-in and distinct wash-out for the yellow selection while the purple ROI is showing moderate enhancement and a plateau.

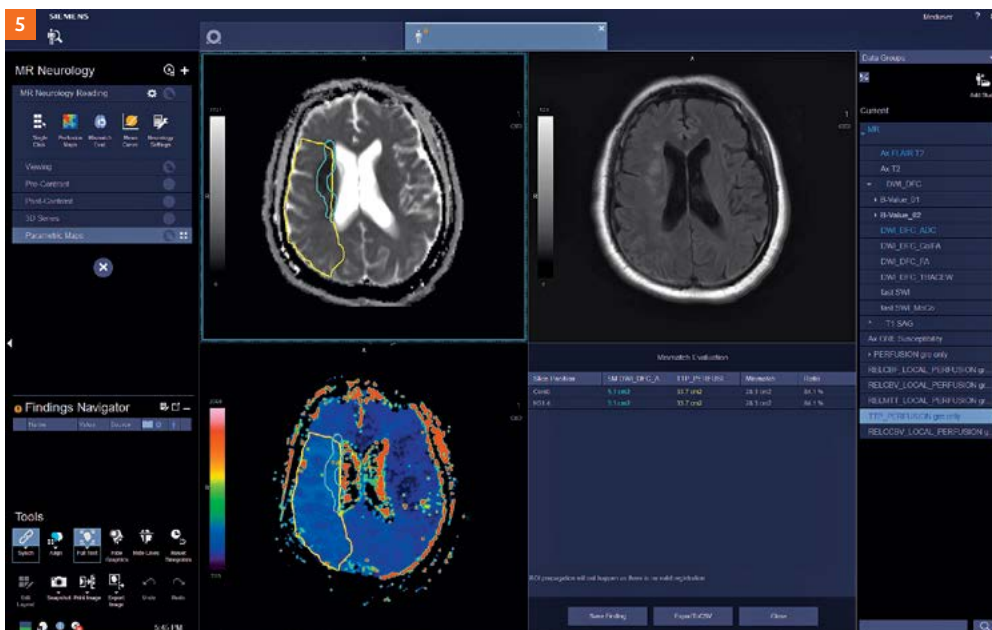
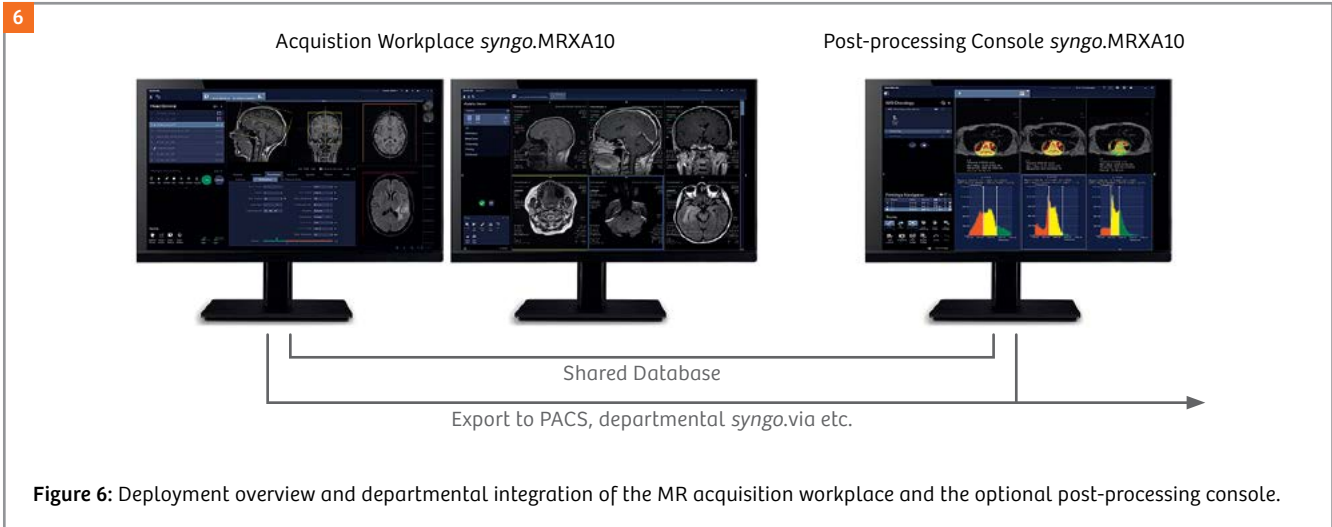


Figure 5: The standard MR Neurology workflow can be enhanced with the capability to perform mismatch evaluation. As shown, the penumbra (yellow outline) is substantially larger than the core infarction (turquoise area) in this patient, prompting immediate treatment.



Advanced image processing

For more advanced image processing requirements, e.g. to perform neuro perfusion and mismatch analysis (Fig. 5), dedicated applications are optionally available. These applications cover the entire radiological spectrum from neurology (MR Neurology, Neuro3D Tractography and fMRI), cardio-vascular evaluations, Cardiac Flow, 4D Ventricular Function, Vascular Analysis), to oncology (Breast, Prostate, OncoCare, 3D Lesion Segmentation)¹. Many of these only require minimal user interaction: for example, flow quantification is fully automated after a vessel has been selected for analysis. This allows preparing MR datasets ready-to-read, saving one of the most precious resources: the radiologists' time. Depending on the institutional setup and needs, it is also possible to operate a satellite console with a shared database for basic (MR View&GO) and advanced processing purposes (Fig. 6). This configuration has the particular advantage that licenses for advanced applications are shared between the acquisition workplace and the satellite console.²

Finally, the appearance and usability of all applications has been harmonized with our departmental post-processing platform syngo.via, helping to improve workflow efficiency.

Summary

The new user interface syngo MR XA10 is designed to improve the technologist's user experience with clearly separated tasks following the natural flow of their work. This not only helps to make routine exams more comfortable to perform and focus more on the patient than on the machine, but also supports in cases where rapid results are decisive. For example in imaging of acute stroke the combination of highly optimized exams using GOBrain, which only needs 5 minutes acquisition time, together with subsequent mismatch analysis (Fig. 5) right at the scanner can save precious time and may help to gain therapy-relevant information faster.

Reference

¹Anderson, JA; et al. CIC Report 200311.

Contact



Gregor Thörmer, Ph.D.

Global Segment Manager
MR Imaging in Oncology

Siemens Healthcare GmbH
HC DI MR CRM AW
Phone: +49 (9131) 84-7726
gregor.thoermer@siemens-healthineers.com

¹This reflects only a selection of advanced applications, further options are available.

²Only one user can process data at a time with one license.

The entire editorial staff at University Hospital Tübingen and at Siemens Healthineers extends their appreciation to all the radiologists, technologists, physicists, experts, and scholars who donate their time and energy—without payment—in order to share their expertise with the readers of MAGNETOM Flash.

MAGNETOM Flash – Imprint

© 2017 by Siemens Healthcare GmbH,
All Rights Reserved

Publisher:

Siemens Healthcare GmbH
Magnetic Resonance,
Karl-Schall-Str. 6, D-91052 Erlangen, Germany

Editor-in-chief:

Antje Hellwich
(antje.hellwich@siemens-healthineers.com)

Guest Editor:

Professor Konstantin Nikolaou
University Hospital Tübingen
Diagnostic and Interventional Radiology
Hoppe-Seyler-Str. 3
72076 Tübingen
Germany

Editorial Board:

Reto Merges; Wellesley Were; Sunil Kumar S.L., Ph.D.;
Gary R. McNeal, MS (BME)

Review Board:

Lisa Chuah, Ph.D.; Daniel Fischer; Berthold Kiefer, Ph.D.;
Heiko Meyer, Ph.D.; Efrén Ojeda; Gregor Thörmer, Ph.D.

Production:

Norbert Moser,
Siemens Healthcare GmbH

Layout:

Agentur Baumgärtner,
Friedrichstr. 4, D-90762 Fürth, Germany

Printer:

G. Peschke Druckerei GmbH,
Taxenstr. 4, D-85599 Parsdorf b. Munich, Germany

Note in accordance with § 33 Para.1 of the German Federal Data Protection Law: Despatch is made using an address file which is maintained with the aid of an automated data processing system.

MAGNETOM Flash is sent free of charge to Siemens MR customers, qualified physicians, technologists, physicists and radiology departments throughout the world. It includes reports in the English language on magnetic resonance: diagnostic and therapeutic methods and their application as well as results and experience gained with corresponding systems and solutions. It introduces from case to case new principles and procedures and discusses their clinical potential. The statements and views of the authors in the individual contributions do not necessarily reflect the opinion of the publisher.

The information presented in these articles and case reports is for illustration only and is not intended to be relied upon by the reader for instruction as to the practice of medicine. Any health care practitioner reading this information is reminded that they must use their own learning, training and expertise in dealing with their individual patients. This material does not substitute for that duty and is not intended by Siemens Healthineers to be used for any purpose in that regard. The drugs and doses mentioned herein are consistent with the approval labeling for uses and/or indications of the drug. The treating physician bears the sole responsibility for the diagnosis and treatment of patients, including drugs and doses prescribed in connection with such use. The Operating Instructions must always be strictly followed when operating the MR system. The sources for the technical data are the corresponding data sheets. Results may vary.

Partial reproduction in printed form of individual contributions is permitted, provided the customary bibliographical data such as author's name and title of the contribution as well as year, issue number and pages of MAGNETOM Flash are named, but the editors request that two copies be sent to them. The written consent of the authors and publisher is required for the complete reprinting of an article.

We welcome your questions and comments about the editorial content of MAGNETOM Flash. Please contact us at magnetomworld.med@siemens.com.

Manuscripts as well as suggestions, proposals and information are always welcome; they are carefully examined and submitted to the editorial board for attention. MAGNETOM Flash is not responsible for loss, damage, or any other injury to unsolicited manuscripts or other materials. We reserve the right to edit for clarity, accuracy, and space. Include your name, address, and phone number and send to the editors, address above.

MAGNETOM Flash is also available online:

siemens-healthineers.us/vida-flash

MRI that adapts to the patient. No matter who walks through the door.



Patient biovariability creates significant challenges in MRI. Inconsistent exams. Poor image quality. Increased rescan potential. Unpredictable scheduling. They all can negatively impact the quality and cost of the care you provide.

That's why we created BioMatrix, the only technology that adapts to each patient to support greater speed, consistency, and precision in MRI.

Imagine if your scanner could anticipate challenges like limited breath-hold ability, adjust on-the-fly to initiate the optimal scan protocol, and deliver the high-quality

images necessary to support an accurate diagnosis and treat your patients.

It's possible with BioMatrix on the all-new MAGNETOM® Vida 3T scanner.

Embrace human nature in MRI. MAGNETOM Vida with BioMatrix helps you overcome the biovariability challenge to deliver more consistent, cost-effective exams for every patient.

Siemens Healthineers.
Engineering success. Pioneering healthcare. Together.

At Siemens Healthineers, our purpose is to enable healthcare providers to increase value by empowering them on their journey towards expanding precision medicine, transforming care delivery, and improving patient experience, all enabled by digitalizing healthcare.

An estimated 5 million patients globally benefit every day from our innovative technologies and services in the areas of diagnostic and therapeutic imaging, laboratory diagnostics and molecular medicine, as well as digital health and enterprise services.

We are a leading medical technology company with over 170 years of experience and 18,000 patents globally. With more than 48,000 dedicated colleagues in 75 countries, we will continue to innovate and shape the future of healthcare.

The outcomes and statements provided by customers of Siemens Healthineers are unique to each customer's setting. Since there is no "typical" hospital and many variables exist (e.g., hospital size, case mix, and level of service/technology adoption), there can be no guarantee that others will achieve the same results.

On account of certain regional limitations of sales rights and service availability, we cannot guarantee that all products included in this brochure are available through the Siemens Healthineers sales organization worldwide. Availability and packaging may vary by country and is subject to change without prior notice. Some/ALL of the features and products described herein may not be available in the United States.

The information in this document contains general technical descriptions of specifications and options as well as standard and optional features, which do not always have to be present in individual cases.

Siemens Healthineers reserves the right to modify the design, packaging, specifications, and options described herein without prior notice. For the most current information, please contact your local sales representative from Siemens Healthineers.

Note: Any technical data contained in this document may vary within defined tolerances. Original images always lose a certain amount of detail when reproduced.

Siemens Healthineers Headquarters
Siemens Healthcare GmbH
Henkestr. 127
91052 Erlangen, Germany
Phone: +49 9131 84-0
siemens-healthineers.com

Published by
Siemens Medical Solutions USA, Inc.
40 Liberty Boulevard
Malvern, PA 19355-9998, USA
Phone: 1-888-826-9702
siemens-healthineers.us